Highlights

- We propose a new approach to assess thermal maturity of Paleozoic successions
- Data were used to calibrate two thermal models in the Holy Cross Mountains
- A new thermal and burial evolution of the area has been proposed
- New and old dataset were used to build 2D thermal maturity maps at different ages
- Coupling 2D maps and pyrolysis we define the potential of source rocks in the area

Assessment of thermal evolution of Paleozoic successions of the Holy Cross Mountains (Poland)

A. Schito[a], S. Corrado[a], M. Trolese[a], L. Aldega[b], C. Caricchi[c], S. Cirilli[d], D. Grigo[e], A. Guedes[f], C. Romano[a], A. Spina[d], and B. Valentim[f]

[a] Università degli Studi di Roma Tre, Dipartimento di Scienze, Sezione di Scienze Geologiche, Largo San Leonardo Murialdo 1, 00146 Rome, Italy
[b] Università Sapienza, Dipartimento di Scienze della Terra, Piazzale Aldo Moro 5, 00195 Rome, Italy
[c] INGV, Via di Vigna Murata 605, 00100 Rome, Italy
[d] Università degli Studi di Perugia, Dipartimento di Fisica e Geologia, Via Alessandro Pascoli, 06123 Perugia PG, Italy
[e] Eni SpA e Exploration & Production Division, Via Emilia, San Donato Milanese, MI, 20097, Italy
[f] Instituto de Ciências da Terra (Pólo da FCUP) e Departamento de Geociências, Ambiente e Ordenamento do Território, Faculdade de Ciências, Universidade do Porto, 4169-007 Porto, Portugal

Corresponding author.

E-mail address: **andrea.schito@uniroma3.it** (A. Schito).

Keywords: Paleozoic source rocks, thermal maturity, Paleozoic organoclasts, vitrinite reflectance, clay mineralogy, Holy Cross Mountains, Raman spectroscopy, Palinomorph Darkness Index

1 Introduction

Reliable assessments of thermal maturity of sedimentary successions is crucial for evaluating hydrocarbon (HC) generation/expulsion scenarios. Uncertainties in thermal maturity modelling can affect decisions on the development of prospects, especially when aimed at exploring unconventional targets (Hackley et al., 2016). In particular, this happens for lower Paleozoic source rocks, because they are devoid of vitrinite macerals that are, by far, the most reliable organic particles used to assess thermal maturity in the ranges of oil and gas generation (Taylor et al., 1998). However, when vitrinite is absent, reflectance measurements and further chemical investigations can be carried on organoclasts of marine origin (e.g., scolecodonts, chitinozoans, and particularly graptolites, cfr. Bertrand, 1990; Bertrand and Heroux; 1987; Goodarzi and Norford, 1987, 1989; Tricker et al., 1992; Caricchi et al., 2016; Hackley et al., 2016).

During the last years, a great interest in unconventional resources has grown in Poland , which has been envisaged as the most perspective country in Europe for exploration of shale gas (SHIP website, http://www.shale-gas-information-platform.org/). Here the Lower Paleozoic successions preserved, in the subsurface in a wide belt (the “Golden belt”, Fig. 1), extending from the Baltic Sea to the NW, to the Ukraine border to the SE, between the Baltic basin and the Lublin basin, are targets for shale-gas and shale-oil exploration (Caricchi et al., 2016). However, one of the most crucial points for the assessment of HC generation/expulsion scenarios, the evaluation of source rock thermal maturation levels, was incorrect despite the calibration of thermal models in the so called “Golden Belts” benefit of a huge existing dataset of thermal maturity, derived from previous exploration for conventional resources. New thermal data from recently drilled successions evidenced that original scenarios frequently overestimated thermal maturity, bringing to turn the expected gas targets into oil targets (Caricchi et al., 2016; Jäger, 2016).

For this reason, after an initial enthusiasm due to preliminary highly perspective scenarios, based on old thermal maturity datasets, the initial incorrect assessment of thermal maturity brought to reduce exploration investments.

In this framework it arises crucial to test a new rationale to compare and integrate old and new datasets, especially in areas where exploration has been ongoing since long ago. HCM Paleozoic outcrops in Central Poland, to the West of the Golden Belt, provide a unique opportunity to study Paleozoic successions and can be envisaged as analogues for those preserved in the subsurface along the Golden Belt and similar plays around the world (Figs. 1 and 2).

In the HCM, located to the East of the Trans-European Suture Zone (TESZ), well preserved outcrops of Cambrian to Carboniferous sedimentary rocks are exposed as a results of the uplift of the area at the end of Mesozoic times. Many works (Belka, 1990; Marynowski et al., 2001; Narkiewicz, 2002; Szczepanik, 1997, 2001) have unravelled the complex burial and thermal history of the HCM using different datasets of thermal maturity indicators (e.g., Conodont Alteration Index - CAI; Thermal Alteration Index - TAI and vitrinite and other organoclasts reflectance - Ro% and Ro_{org}%), but a comprehensive and fully accepted model has not yet been elaborated. In particular, major uncertainties derive from the lack of widely accepted correlation among thermal indicators (e.g., TAI, CAI, Ro_{org}%) against maximum paleo-temperatures that could lead to contrasting interpretations in the assessment of maturation patterns, and timing of hydrocarbon generation of potential Lower Silurian source rocks (Belka, 1990; Marynowski et al., 2001; Narkiewicz, 2002, 2010; Poprawa et al., 2005). Lower Silurian source rocks have been recently studied by means of organic matter optical analyses and Pyrolysis Rock-Eval (Malec et al., 2010; Mustafa et al., 2015; Smolarek et al., 2014), but these data were not applied as constraints for burial and thermal models.

In this paper, available thermal maturity data from literature have been revised and integrated with new thermal maturity data derived from the analyses of the organic (e.g., Tmax from Pyrolysis Rock-Eval, and vitrinite and other organoclasts reflectance) and inorganic fraction (e.g., illite content in mixed layers illite-smectite) of sediments.

This multi-method approach allowed us to calibrate new thermal models, for the two tectono-stratigraphic blocks in which the geological structure of the HCM is organized: the southern Łysogory and southern Kielce blocks, in order to highlight the burial and thermal evolutionary scenarios since Paleozoic times for both sectors.

The integration of different thermal indicators from the organic and inorganic portion of sediments is proposed to reduce the level of uncertainties in thermal maturity assessment, and can be successfully applied not only to similar Paleozoic source rocks successions in Poland but worldwide.

2 Geological setting

The Paleozoic core of the HCM is made up of Cambrian to Carboniferous marine sedimentary units that were intensely deformed, at least, during the Variscan orogeny, and later on unconformably overlain by a thick Late Permian-Mesozoic continental to marine sedimentary succession, which was inverted during the Laramide deformation and nowadays is totally eroded (Kutek and Głazek, 1972).

The HCM are organized into two distinct tectono-stratigraphic blocks: the southern block (Kielce block, that is a part of the Malopolska block) and the northern block (Łysogòry block), bounded by a deep-seated regional lineament, at least 75 km long, known as Holy Cross Fault (HCF, Figs. 2, 3) whose kinematic history is still matter of debate (Dadlez, 2001; Kutek, 2001).

The Paleozoic sedimentary succession, exposed in both blocks, consists of Cambrian siliciclastic rocks deposited along the SW passive margin of the Baltica continent (Mizerski, 2004). Cambrian sediments are made up of shales, evolving to quartzarenites and sandstones (Narkiewicz, 2002).

Since the Ordovician up to the Carboniferous, sedimentation evolved differently in the two blocks leading to considerable facies and thickness variations. These differences have been related by some authors (Dadlez et al., 1994; Narkiewicz, 2002) to different paleogeographic positions for the two blocks in Lower Paleozoic times, whearas Mizerski (2004) and Jaworowski and Sikorska (2006) indicate that facies and thickness variations could be related to differential vertical components of motion along the HCF.

In the Kielce block, Ordovician clayey and silty marine deposits lie with a sharp angular unconformity over the Lower to Middle Cambrian rocks (Figs. 2 and 3; Konon, 2007; Kozłowski, 2008; Kozłowski et al., 2014; Narkiewicz, 2002; Schätz et al., 2006; Urban and Gągała, 2008), and are covered by Lower Silurian graptolitic shales (Kozłowski, 2008), Ludfordian greywackes (Niewachow Beds, Fig. 3; Kozłowski et al., 2014) and Kielce Beds sandstones. Locally, in the Bardo syncline and in Gruchawa area, the Miedziana Góra Conglomerate occurs (Kozłowski et al., 2014; Figs. 2 and 3). Devonian sediments (Pragian-Emsian) are composed of sandstones, and of shallow marine carbonate deposits (Narkiewicz and Narkiewicz, 2010), which unconformably overlie Silurian and/or locally Cambrian rocks (Kowalczewski, 1974). Lower Carboniferous marine marly and clay rocks crop out only at the core of a series of Variscan folds in the northern portion of the Kielce block, close to the HCF (Fig. 2).

In the Łysogóry block, no unconformities occur at the base of Ordovician rocks, over which Llandoverian-Wenlockian graptolitic shales lie (Kozłowski 2008, 2014; Narkiewicz 2002). Niewachow Beds are represented in the Łysogóry block by lithic arenites and shales of the Trzcianka Formation (Fig. 3) which are overlain by a shaly-silty succession of the Trochowiny Formation (Kozłowski, 2008). Unlike the Kielce block, in the Łysogóry block, the Ludfordian greywackes are covered by a thick succession of clastic sediments representing a continuous Late Ludlovian-Lochkovian succession of the Caledonian foreland basin (Narkiewicz, 2002). This late Silurian-Early Devonian succession is composed of the Pridoli Bronkowice/Sarnia, Podchelmie and Rudki Formations and by the Lochovian Bostow formation (Fig. 3). Middle to late Devonian carbonate deposits conformably lie on top of the clastic formations (Szulczewski et al., 1996).

The role of different orogenetic cycles affecting the Cambrian to Carboniferous succession of the HCM is still matter of debate. The primary role played by the Variscan deformation to explain the present day tectonic setting is generally recognized (Lamarche et al., 1999; Mizerski, 2004) with a pre-Late

Carboniferous compression causing a polyphase folding associated with a dominant N-S to NNW-SSE shortening (Lamarche et al., 1999). In addition, an Early Caledonian deformation was detected by Gągała (2015) in the Lower and Middle Cambrian rocks in the Kielce block, but not all authors (e.g Lamarche et al., 1999, Konon, 2007) agree with this piece of evidence.

During Late Permian and Mesozoic times, the HCM were part of the Polish Rift Basin (Kutek, 1974, 2001; Lamarche, 1999; Mizerski, 2004). As a consequence, in the Łysogóry and Kielce blocks, the Cambrian to Devonian/Carboniferous successions were unconformably covered by a Late Permian-Early Triassic continental clastic succession (Konon, 2004; Kozłowski, 2008), evolving to marine sediments in the Late Cretaceous (Konon, 2004.). This succession records as a whole a complex subsidence history ruled by an initial Late Permian-Early Triassic crustal thinning that was followed by two episodes of tectonic subsidence. The Oxfordian-Kimmeridgian episode has been interpreted as corresponding to a second extensional event, whereas the Cenomanian is considered as a precursor of compressional deformation in the basin which culminated in the Laramide basin inversion in Maastrichtian and Paleocene times (Dadlez et al., 1994), with the formation of the Mid-Polish Anticlinorium (Kutek, 2001) and the exhumation of Palaeozoic strata (Konon, 2004; Mizerski, 2004).

3 Materials and Methods

3.1 Materials

Analyzed samples are located in Figure 2 and listed in Table 1. Suitable samples for X-ray diffraction analyses of fine grained sediments and optical, TOC and pyrolysis analyses of kerogen, mainly derive from shaly, silty and organic matter rich beds.

3.1.1 Kielce block

In the Kielce block, 17 samples range in age from Cambrian to Devonian.

Cambrian interval was sampled in the southern portion of the Kielce region, in correspondence of outcropping brownish siltstones (sample 7.1, Fig. 2).

Upper Ordovician to lower Ludlow samples were mainly collected in the Bardo syncline. In detail, sample 5.4 is from the Zalesie Formation (Upper Ordovician sandy mudstones with subordinate shales and sandstones) and three samples (5.1, 5.2, 5.3) are from the Llandovery light brown shales in the southern limb of the syncline from the outcrop of Bardo Stawy locality. Further Silurian samples (4.1, 4.2, 4.3a, 4.3b, 4.4and 4.5) were collected along the northern limb of the Bardo syncline, where upper Wenlock graptolitic shales and mudstones and lower Ludlow graptolitic shales crop out. In the western portion of the Kielce region, near the HCF sample 19.1 comes from the Llandovery graptolitic shales cropping out at the top of the Ordovician glauconitic sandstones.

Devonian samples range in age from Givetian to Famennian. Samples 16.1 and 16.2 were collected from mudstones in the Mogiłki quarry, near the Gruchawka area. Sample 15.1 comes from a Frasnian shaly intervals interbedded in dark limestones in the Kostomłoty hill, to the south of Kielce town. Sample 20.1 derives from the shaly intercalations in cherty-rich mudstones at the Frasnian-Famennian boundary.

3.1.2 Łysogory *block*

In the Łysogory region, 11 samples range in age from Cambrian to Devonian.

The Cambrian interval was sampled close to the HCF, where weakly metamorphosed black shales (1.1 and 1.2), interbedded with shaly mudstones and limestones, crop out.

The Ordovician-Silurian interval was sampled in correspondence of the Bodzentyn syncline and the Bronkowice-Wydryszów anticline (Bodzentyn area, Fig. 2 a). In detail, shaly intervals of the turbiditic successions of the Ludlow-Přídolí Winnica formation (10.1) and of the lower Ludlow Trzcianka Formation (13.1) derive only from the southern limb of the Bodzentyn syncline. In the Bronkowice-Wydryszów anticline four shaly intervals were sampled: two, belonging to the lower Ludlow Trzcianka Formation (12.1 and 12.2) and two to the upper Ludlow Trochowiny Formation (11.1 and 11.2).

Devonian samples derive from the core of the Bodzentyn syncline, to the north of Nowa Słupia town, where sample 8.1 was collected from Eifelian mudstones, sample 9.1 from Givetian-Frasnian siltstones. In addition, sample 2.1 derive from black shales cropping out to the north of the HCF (Fig. 2 a).

The Mesozoic successions were sampled in two localities. Sample 14.1 belongs to Triassic reddish sandstones, whereas samples 17.1, 17.2, 17.3, 17.4, 17.5 and 18.1 come from the Jurassic deposits that crop out to the NW (sample 18.1) and to the N (samples 17) of the Paleozoic core (Fig. 2b).

3.2 Methods

3.2.1 Geospatial analyses

Thermal maturity data derived from previous studies have been organized into a GIS database, including vitrinite reflectance (R_o%), vitrinite reflectance equivalent (R_o% eq.) from reflectance measured on graptolites or other organoclasts, Conodont Alteration Indexes (CAI). The data were plotted using the Kernel smoothing tool in ArcGis. This tool allowed to:

i) quantify the spatial variation of distribution pattern of point values using semivariograms;

ii) introduce discontinuities in the spatial interpolation, that in this case history is represented by the HCF.

3.2.2 Clay mineralogy

Clay minerals in shales and sandstone undergo diagenetic and very low-grade metamorphic reactions in response to sedimentary and/or tectonic burial. Reactions in clay minerals are irreversible under normal diagenetic and anchizonal conditions, so that exhumed sequences generally retain indices and fabrics indicative of their maximum thermal maturity and burial. Mixed layers illite-smectite (I-S) are widely used in petroleum exploration as a geothermometer, and as an indicator of the thermal evolution of sedimentary sequences (Aldega et al., 2014; Hoffman and Hower, 1979; Pollastro, 1990;). In this study, qualitative an semiquantitive XRD analyses of the whole rock composition and of the<2 μm grain size fraction were performed on the same dataset (28 samples), accordingly to the procedure of Giampaolo and Lo Mastro (2000) and following Moore and Reynolds' recommendations (1997). XRD analyses have been carried out with a Scintag X_1 X-ray system (CuKα radiation, solid-state detector, spinning sample) at 40 kV and 45 mA. Randomly oriented whole rock powders were run in the 2-70° 2 θ interval with a step size of 0.05°2θ and a counting time of 3s per step. Oriented mounts were prepared by the pipette-on-slide method and analyzed in the air-dried and ethylene-glycol solvated forms (saturation in ethylene-glycol atmosphere at room temperature for 24 h) in the 1 to 48°2θ and a 1 to 30°2θ ranges respectively with a step size of 0.05°2θ and a counting time of 4 s per step.

The illite content in mixed-layer illite-smectite (%I in I-S) was determined by the Δ2θ method after decomposing the composite peaks between 9-10°2θ and 16-17°2θ (Moore and Reynolds, 1997) and by modeling X-ray diffraction patterns using the Scintag X_1 software program with Pearson VII functions.

The I-S ordering type (Reichweite parameter, R; Jagodzinski, 1949) was determined by the position of the illite 001/S 001 reflection between 5 and 8.5°2θ (Moore and Reynolds, 1997). Integrated peak areas were transformed into mineral concentration by using mineral intensity factors as a calibration constant (Moore and Reynolds, 1997).

Non-clay minerals were not taken in account in the <2 μm grain-size fraction quantitative analysis, thus, the given data refer to the phyllosilicates group only. The amounts of clay minerals in the analyzed clay-size fraction were not recalculated into percentages of bulk rocks but represent the content of the specific separated phyllosilicate-size fraction.

3.2.3 Pyrolisis Rock-Eval and TOC

Pyrolisis Rock-Eval is a quantitative analysis for kerogen characterization based on the evaluation of the amount of hydrocarbon artificially generated. Three fluid peaks (S1, S2 and S3) produced during thermal cracking are related to hydrocarbons already generated in nature, the residual potential of the source rock, and the amount of CO_2 expelled during the pyrolysis. The Hydrogen Index (HI), defined as the ratio between S2 peak and Total Organic Carbon (TOC), allows to know the kerogen type. In addition, the relationship between hydrocarbons produced and the residual potential (S1/S1+S2, known as the transformation ratio) is analyzed to evaluate the productive potential of the source rock.

Total organic carbon (TOC) refers to the weight percent (wt %) of the organic carbon present in 100g of rock (Langford and Blanc-Valleron, 1990).

Rock Eval and TOC measurements were perfomed using a Rock-Eval 6 equipment.

3.2.4 Organic matter optical analyses

Vitrinite derives from thermal degradation of huminite-vitrinite group macerals (i.e., woody tissues of vascular plants) that can be dispersed in sediments (e.g., Stach et al., 1982; Teichmüller, 1987) and its transforming reactions are not reversible with exhumation and/or temperature decrease. Therefore, vitrinite reflectance (R_o%) is the most widely used quantitative parameter to determine the dispersed organic matter thermal maturity levels in hydrocarbon exploration, as it is correlated with thermal evolution of host sediments, and provides consistent and reliable information on maximum burial depths (Corrado et al., 2009; Meneghini et al. 2012; Carlini et al.; 2013).

Although widely used and well known, this parameter cannot be measured on sediments older than Lower Paleozoic, because of the absence of wooden terrestrial material until the Silurian advent of continental floras. However, in sedimentary sequences that are lacking of vitrinite macerals, thermal maturation can be evaluated measuring reflectance on marine organoclasts (e.g. graptolites) (Bertrand and Malo, 2012, Petersen et al., 2013; Schmidt et al., 2015; Xianming et al., 2000). Therefore, in this work, the organic matter maturation was determined using both vitrinite and graptolite reflectance according to ASTM D7708-14.

Before reflectance measurements the samples were prepared according to Bustin et al. (1989) standard procedure, and the vitrinite and organoclasts reflectance was measured under oil immersion (ne 1.518, at 23ºC), with a Zeiss Axioskop 40, with a tungsten-halogen lamp (12V, 100w), an Epiplan-Neofluar 50x/1.0 oil objective, in incident filtered (λ = 546 nm) monochromatic non-polarized light. The microscope is equipped with the MPS 200 detection system by J&M Analytik AG.

On each sample, about 20 measurements have been carried out on well-preserved or slightly fractured vitrinite or graptolite fragments and other organoclasts. Mean reflectance values (R_o%) were calculated from the arithmetic mean of each measurement set. In the analyzed Paleozoic successions, reflectance analyses have been carried out mainly on graptolites. However, in some cases the origin of fragments was uncertain and the term vitrinite-like fragment and Ro_{org}% were adopted.

Thereafter, vitrinite equivalent reflectance values (Ro_{eq}%) were obtained from graptolite and vitrinite-like fragments reflectance values using three different equations by Xianming et al. (2000); Petersen et al. (2013) and Schmidt et al. (2015).

These formulas are:

$Ro_{eq}\% = 1.26\ Ro_{org}\% + 0.21$ (when $Ro_{org}\% < 0.75$, Xianming et al., 2000, Eq. 1)

$Ro_{eq}\% = 0{,}28\ Ro_{org}\% + 1.03$ (when $Ro_{org}\% > 0.75$, Xianming et al., 2000, Eq. 2)

$Ro_{eq}\% = 0.73\ Ro_{org}\% + 0.16$ (Petersen et al., 2013, Eq. 3)

$Ro_{eq}\% = 0.9916\ Ro_{org}\% + 0.1590$ (when $Ro_{org}\% < 0.75$, Schmidt et al., 2015, Eq. 4)

$Ro_{eq}\% = 0.9046\ Ro_{org}\% + 0.3786$ (when $Ro_{org}\% > 0.75$, Schmidt et al., 2015, Eq. 5)

3.2.5 Raman spectroscopy on kerogen

Raman spectroscopy is a powerful and promising tool for the analysis of dispersed organic matter in metamorphism and diagenesis (Beyssac et al., 2002; Guedes et al., 2010, 2012; Lahfid et al., 2010; Liu et al., 2012; Wilkins et al., 2014). It is based on an inelastic light scattering process in which the frequencies of the scattered photons are shifted from those of the incident photon frequencies according to the vibrational modes of the molecule or atomic group (Dubessy et al., 2012).

Raman spectrum on dispersed organic matter is composed by two main bands called the D and the G bands, associated respectively with disordered and ordered structures in the organic matter, and by other minor bands depending on the degree of structural ordering (Beyssac et al., 2002; Lahfid et al., 2010; Li et al., 2007; Schito et al, 2016). The shape of the Raman spectra has been found to change as a response of an increase in maturation caused by the increase in paleotemperatures during progressive burial. In detail, during graphitization, these changes can be quantified by the intensity ratio of the D and G bands (Ferrari and Robertson, 2000, 2004; Wopenka and Pasteris, 1972), whereas in epizone, anchizone and diagenesis, successful parametrization has been found using the area ratio of the two main bands and the minor bands (Beyssac et al., 2002; Guedes et al., 2010; Lahfid et al., 2010).

In this work we performed Raman analyses on three samples from Cambrian units collected in both the Łysosgory and the Kielce blocks. We performed analyses on concentrated kerogen used a Jobin Yvon micro-Raman LabRam system in a backscattering geometry, in the range of 700-2,300 cm−1 using a 600 grooves/mm spectrometer gratings and CCD detector under a maximum of 100X optical power.

A laser source Neodimium-Yag at 532 nm (green laser) was used as the light source and optical filters adjusted the power of the laser (<0.6 mW). The Raman backscattering was recorded after an integration time of 20s for 6 repetitions for each measure. Each organic grain was analysed focusing an illuminated spot of about 2 μm with a 50× objective lens.

Spectra were deconvoluted using LabSpec software in order to determine frequencies, bandwidths and the relative intensities of bands. High ordered spectra collected in the Lysogory region were deconvoluted using a pure Lorentzian five peaks curve-fitting according to the procedure described by Lahfid et al. (2010), while spectra from samples collected in the Kielce region were deconvoluted according to a mixed Gaussian-Lorentzian six peaks decomposition according to Guedes et al., (2010).

3.2.6 Palynomorph Darkness Index (PDI)

Recently Goodhue and Clayton (2010) proposed a new quantitative method to establish the thermal maturity of organic matter: Palynomorph Darkness Index (PDI). It is a relatively simple method that utilizes a transmitted light microscope with digital imaging capacity and software capable of simple image analysis. PDI is determined fro measurement of the red, green and blue (RGB) intensities of light transmitted through palynomorphs to produce a single greyscale value. Goodhue and Clayton (2010) demonstrated a progressive increase of PDI with increasing temperature, suggesting that the technique is applicable through a broad temperature range.

For PDI analysis, organic matter was concentrated from two samples (e.g. 4.4 and 5.3) using palynological standard techniques. The samples were treated by acid maceration (HCl 37% and HF 50%) and filtration of the organic-rich residue at 10 μm.

Light microscope observations were performed on palynological slides using a Leica DM 1000 microscope with Differential Interference Contrast technique in transmitted light. Images were captured with the digital microscope camera and successively processed for PDI determination using ImageJ public domain software (imagej.net).

In this study, twenty specimens from each sample of unornamented palynomorphs (e.g. prasinophytes as Tasmanites spp.) were considered for determination of PDI (i.e. PDI Tasmanites, Fig. XX). The measuring area of approximately 50 μm^2 was used with a x100 magnification. For each palynomorph, the RGB intensities of 10 different areas were measured and the PDI calculated.

3.2.7 Thermal modelling

In order to model the burial and thermal evolution of the two tectonic blocks, we simulated two pseudo-wells, roughly corresponding to the stratigraphic successions detected along the Bardo syncline for the Kielce block and along the Bodzentyn syncline for the Łysogóry block. The two pseudo-wells were built according to Oncken's (1982) and Nöth et al.'s (2001) method, using thicknesses measured in the field or derived from previous works (Kozłowski, 2008; Gągała, 2015; Trela, 2007):

In the Kielce block, the Ordovician is composed by 200m thick black shales in the SW sector and, locally, by 50m of limestones (Trela, 2007), whereas the Silurian section is composed of 300m thick black shales that deposited between Llandovery and Lower Ludlovian, overlain by about 1,500m of Ludlovian greywackes (Fig. 3). During the Pridolian, only few meters of the Miedziana Gora conglomerates sedimented (Kozlowsky, 2008). Devonian deposits made up of about 200m thick Emsian sandstones, 300m of Eifelian limestones and about 750m of Givetian to Fammenian mudstones and shales unconformably overlie the Silurian succession. Carboniferous deposits are composed by 400m thick shales (measured in the Gałęzice G-5 well).

Thicknesses values for the Mesozoic successions are from Brzegi IG-1 and Brzescie 4 wells, located to the south of the Kielce block with 850m of Upper Permian-Triassic sandstones, about 830 m of Kimmerdigian to Bathonian limestones and about 600m of Maastrichtian to Albian marls.

Concerning the Lysogory region, Ordovician succession is composed of 250m thick shales, and overlain by 300m of Landoverian to Lower Ludlovian black shales and 1450m of Ludlovian to Lower Lochkovian greywackes (Kozłowski, 2008). The Devonian succession is composed of 800m thick Lochkovian to Emsian sandstones, 700m thick Eifelian limestones and Givetian to Fammenian 750m thick marls (Kozłowski, 2008; Gągała, 2015). Mesozoic successions are thicker than those observed in the Kielce block and are composed of 1,500m thick Upper Permian - Triassic sandstones (measured in the Radoszyce 3 well), 1,500m of Kimmerdgian to Hettangian marls (Ostałow PIG-2 well) and about 930m of Cretaceous marls (Lisow 1 well).

For both models, two phases of exhumation were recognised: an older one between Late Carboniferous and Early Permian and associated with the unconformity at the base of Upper Permian succession recorded in the whole area, and a younger one between Maastrichtian and Paleogene associated with the so-called "Laramide" event of the mid-Polish though that brought to its positive inversion (Dadlez et al., 1994; Konon, 2004; Lamarche et al., 1999).

Data on present-day heat flow of 46 and 49, respectively for the Kowala 1 and Janczyce 1 wells, derive from Narkiewicz's work (2002).

Simplified reconstructions of the burial and thermal history of the Ordovician-Devonian successions have been performed using the software package Basin Mod® 1-D (1996). The main assumptions for modeling are that: (1) rock decompaction factors apply only to clastic deposits, according to Sclater and Christie's method (1980); (2) seawater depth variations in time are assumed as not relevant, because thermal evolution is mainly affected by sediment thickness rather than by water depth (Butler, 1992); (3) thermal modeling is performed using LLNL Easy%R_o method, based on Burnham and Sweeney (1989) and Sweeney and Burnham (1990); 4) a surface temperature of 10°C and (5) variable heat flow values through time (35 mW/m^2 during Paleozoic and 45mW/m^2 from Triassic onwards.

Rock properties including initial porosity, compaction data, density, conductivity and heat capacity, were chosen from the software libraries between those available for pure or mixed lithologies.

Illite content in mixed layers I-S was converted into Ro% equivalent values on the base of the correlations between these two indicators according to Aldega et al. (2007) and Merriman and Frey (1999).

4 Previous thermal maturity data

4.1 Cambrian and Ordovician

Thermal maturity indicators from Cambrian successions mainly come from Szczepanik's works (1997) who carried out analyses on alteration colours of acritarchs using the TAI scale after AMOCO modification (Szczepanik, 1997). The same values were presented by Narkiewicz (2002) and expressed as CAI values, in order to be compared with other thermal maturity indicators. These data are from a series of shallow boreholes, mainly not deeper than 500m. Data expressed as CAI values (Narkiewicz, 2002) show different thermal maturity for the two blocks. As matter of fact, CAI values in the Kielce block range between 1 and 2 indicating the immature stage of HC generation, whereas in the Łysogóry block they indicate the mature stage with CAI values ranging between 3 and 5 (Fig. 4a).

4.2 Silurian

Thermal maturity of Silurian graptolites-bearing shales have been assessed by CAI values reported in Narkiewicz (2002), and by reflectance measurements performed on vitrinite-like macerals by Smolarek et al. (2014).

Samples are from boreholes and outcrops from the Llandovery to Ludlow time span.

There are only two CAI values from the Kielce block which show low thermal maturity (1.5) in the Bardo syncline, and 4, close to the HCF (Fig. 4b). Values from graptolites reflectance analyses and/or other organoclasts ranging from 0.7 to 1.7 R_o and R_o eq. % (Fig. 4b; Smolarek et al., 2014) with a generally increase of maturation from north to south in the HCM area (Smolarek et al., 2014).

4.3 Devonian

Organic matter optical analyses on Devonian rocks have been widely performed in the Kielce block, where limestones and shales are exposed in several quarries, while in the Łysogóry block data are from the Eifelian sandstones and Emsian shales in the northernmost part of the region (Belka 1990).

Thermal maturities pertaining to the early mature stage of HC generation were measured in the south-western part of the Kielce region where Famennian to Eifelian limestones and dolostones crop out or are reached by drillings. Here vitrinite reflectance values ranges between 0.55 % for the Frasnian black shale in the Kowala quarry, to 0.67 R_o% for the Eifelian dolostones, collected from the Kowala-1 borehole (Marynowski et al., 2001; Rospondek et al., 2008). Moving toward the NE, vitrinite reflectance values range between 0.74 and 1.20 R_o% along the HCF, where shales and dolostones from the Givetian to Frasnian crop out.

In the Łysogóry block, Devonian successions are exposed only in the northern part, close to the town of Bodzentyn. Thermal maturity of these rocks was assessed by means of R_o% (Belka, 1990;), showing values of about 1.15.

5 Results

5.1 Clay mineralogy

X-ray diffraction results for the whole-rock composition and the < 2 μm grain-size fraction of Cambrian to Jurassic samples of both tectonic blocks are shown in Table 2, and are plotted in Figure 5.

Randomly oriented whole-rock powder patterns of Cambrian samples in the Łysogóry region are composed mainly of phyllosilicates (73-76%) and quartz (18-23%) with subordinate amounts of plagioclase (3-4%) and k-feldspar (1-2%). The <2 μm grain-size fraction contains illite (91%) as major mineral and subordinate amounts of rectorite, kaolinite, chlorite and pyrophyllite.

The whole-rock mineralogical assemblage of the Cambrian sample collected in the Kielce block is made up of phyllosilicates (76%), quartz (13%), plagioclase (10%) and minor amounts of hematite (1%). The <2μm grain size fraction shows illite as the principal component (72%), and subordinately mixed layers illite-smectite (10%), chlorite-smectite (17%) and low amounts of chlorite (1%). Mixed layers illite-smectite are composed of two populations of illite-smectite crystals characterized by short-range and long-range structures with low expandability (R1-R3 I-S with an illite content of 77%).

Ordovician samples from the Bardo syncline, in the Kielce region, are mainly characterized by phyllosilicates and quartz, which constitute 96%-97% of the overall composition. Plagioclase, hematite (in sample 6.1) and K-feldspar (in sample 5.4) occur as minor phases. Illite, mixed layers I-S and kaolinite are the occurring minerals in the <2 μm grain-size fraction. Non-clay minerals such as quartz and k-feldspar are also observed in this fraction. Mixed layers illite-smectite are composed of long-range structures (R3) with an illite content of 83%.

Llandovery shales are mainly composed of phyllosilicates (56-79%), quartz (17-40%) and minor amounts of plagioclase (3-7%). Locally, goethite and k-feldspar occur in the sediments. Among the phyllosilicates in the <2 μm grain-size fraction, illite, mixed layers illite-smectite and chlorite occur. Small amounts of kaolinite and mixed layers chlorite-smectite have been identified in sample 5.3. Mixed-layered clay minerals consist of short range ordered structures (R1) with an illite content of 77% or long range ordered (R3) with an illite content of 83%.

Ludlow-Wenlock samples in the Kielce region display a whole-rock composition made of phyllosilicates (62-79%), quartz (12-17%), plagioclase (7-12%) and low amounts of calcite (<6%) and k-feldspar (1%). Occasionally, small contents of dolomite and pyrite (<2%) occur. The <2 μm grain size fraction is mostly composed of illite (55-69%) and subordinate amounts of chlorite (2-22%), mixed layers I-S (2-19%) and C-S(8-17%) and kaolinite (<5%). Mixed-layered clay minerals generally consist of long-range ordered I-S with an illite content between 80% and 83% and mixed layer C-S with a chlorite content ranging from 60% to 80%.

Ludlow silty shales in the Łisogory block are characterized by phyllosilicates (78-89%), quartz (5-16%) and albite (2-6%). Low amounts of hematite (1-3%) occasionally occur. Oriented mounts of the <2 μm grain size fraction display mostly illite-rich assemblages, which constitute at least 58% of the overall composition, and subordinate amounts of chlorite, kaolinite and mixed-layered minerals (Table 2). Discrete smectite has been detected in sample 13.1 and could be interpreted as result of “retrograde diagenesis” (Nieto et al., 2005). Mixed layers I-S are long-range ordered (R3) structures with an illite content between 85 and 88%. Mixed layers chlorite-smectite show a chlorite content ranging between 54 and 78%.

Givetian to Famennian samples collected in the Kielce block are composed of high amounts of carbonate group minerals (calcite, dolomite and ankerite) and phyllosilicates, and subordinate amounts of quartz (2-7%) and albite (1-2%). Occasionally, K-feldspar and pyrite occur (Table. 2). Oriented mounts show an illite-rich assemblage (79-85%) with subordinate amounts of chlorite (8-14%) and mixed layers I-S (7-15%). Observed I-S corresponds to low expandability R3 or R1-R3 (in sample 20.1) structures where the illite component is dominant (80-85%). In the Eifelian-Frasnian samples from the Łisogory block, phyllosilicates constitute at least 72% of the overall composition, followed by quartz (2-10%) and occasionally by calcite, ankerite and albite. Among clay minerals, illite (59-95%) prevails over kaolinite (1-27%) and mixed layer I-S (1%-16%). The I-S corresponds to R3 structures with an illite content of 82-84%.

The Triassic portion of the succession is characterized by quartz (34%), phyllosilicate minerals (58%) and small contents of hematite (6%) and plagioclase (2%). Among the phyllosilicates in the <2 μm grain-size fraction, an illite-rich assemblage (78%) occur with subordinate kaolinite contents (14%) and small amounts of long-range ordered mixed layer I-S (5%) and chlorite (3%).

Samples from the Jurassic successions are mainly composed of quartz and phyllosilicates and low amounts of K-feldspar and plagioclase that never exceed 4%. In the <2μm grain size fraction illite and kaolinite are the most abundant minerals followed by mixed layers I-S and chlorite (Tab. 2). Mixed layers I-S are R1 structures with 65% of illitic layers or R1-R3 structures with an illite content of 75%.

5.2 TOC and Pyrolysis Rock-Eval

TOC measurements and Pyrolysis Rock-Eval data are listed in Table 3. TOC content for most samples is generally low and below 1%. In particular, samples from the Łysogory block show values lower than 0.5%. In the Kielce region, TOC contents higher than 1% are those from Wenlock-Ludlow, Llandoverian and Ordovician intervals collected in the Bardo syncline (Fig. 6) and from Middle Devonian samples that show high TOC values of 4.57 and 9.17% respectively for samples 16.1 and 16.2.

Jurassic rocks also show very high TOC with a maximum of 5.89 for sample 18.1.

Results from Pyrolysis Rock-Eval show a general low potential except for sample 16.2 that shows S1 and S2 values indicating a good potential (respectively higher than 1 and 5).

Hydrogen indexes (HI) indicate gas prone sources ($0 < HI < 150$) in almost all samples and gas and oil prone sources ($HI > 150$) only for samples from the Bardo syncline (4.3b. 5.1 and 5.2) and the Jurassic succession.

Tmax values are between 437 and 441°C in the Ordovician-Silurian succession of the Bardo syncline, indicating the oil window, whereas the gas window was achieved in sample 16.1 (Tmax > 470°C). Jurassic samples show Tmax values between 433 and 439 suggesting the immature to early mature stage of hydrocarbon generation. Samples 19.1 and 20.1 show Tmax values of 442 and 441°C respectively, indicating mid mature stages of HC generation.

Looking at the HC generation potential of analysed samples, we can see that Silurian, Jurassic, and in minor account Devonian kerogen, shows values indicative of source rocks with fair to good HC generation potential (Fig. 6).

5.3 Optical analysis on the Organic matter: graptolites, vitrinite-like and vitrinite reflectance data

As shown in Table 3, samples from Cambrian rocks are poor in organic carbon (TOC < 1%). The measurement of the reflectance of the organic matter in the bulk rock was not reliable since the organic fragments were generally oxidized. However, petrography of the concentrated organic matter of samples 1.1 and 1.2 from the Łisogory block, shows that kerogen is mainly composed by fragments with reflectance values ranging between 2 and 5 Ro_{org}% (Fig. 7a), and by rare fragments with reflectance values higher than 10 (Ro_{org}%), corresponding to anthracite-graphite stages (Fig. 7b). Conversely sample 7.1 (Cambrian rock outcropping in Kielce block) shows lower reflectance values (1.06 Ro_{org}%, measured on highly oxidized organic matter).

Ordovician samples collected from the Bardo syncline, in the Kielce block, are very poor in organic matter content. The more reliable reflectance results come from the concentrated kerogen from sample 5.4 where most of the fragments have been recognized by their small and elongated shape as graptolite fragments with 1.07 Ro_{org}%. These fragments show their rims covered by small globular pyrite aggregates.

Samples from Silurian rocks are very rich in well-preserved organic matter, which provided highly reliable Ro_{org}% data with generally tens of analyzed fragments per sample resulting in a Gaussian distribution of measurements that represent the indigenous population of marine organoclasts. Identified graptolites were found to occur as gray elongated thin fragments without internal granulated texture (Fig. 8).

Llandovery samples have been collected in the Kielce block and indicate a mean value of Ro_{org}% ranging between about 0.70 and 1.04 (Table 4).

In Wenlock interval of the southern block, sample 4.4 has 0.92 Ro_{org}% and sample 4.5 has 0.89 Ro_{org}%, whereas in the northern block the Ro_{org}% value increases up to 1.55 in sample 13.1 (Table 4).

In samples 4.1, 4.2, 4.3a and 4.3b of the Ludlow interval of the southern block, reflectance values increase from 0.69 Ro_{org}% for the youngest sample (4.1) to 0.95 Ro_{org}% for the oldest one (4.3.b). In contrast, samples 10.1, 11.1, 11.2 and 12.1, collected in the Łysogory block show higher reflectance values ranging between 1.62 Ro_{org}% and 1.68% Ro_{org}% (Table 4).

Devonian samples in the Kielce block close to the HCF, show very high reflectance values ranging from 1.12 Ro_{org}% to 1.95 Ro_{org}% respectively for samples 16.1,16.2 and 15.1. However, sample 20.1, which located ca. 20 km SE of these, shows a value of 0.8 Ro_{org}%.

In the Łysogory block, Devonian samples show a reflectance value of 0.84 Ro_{org}% for Eifelian rocks (sample 8.1) and 1.08 Ro_{org}% and 0.92 Ro_{org}% for Givetian/Frasnian successions (samples 9.1 and 2.1, respectively).

In three samples of the Jurassic outcrops clearly recognizable vitrinite fragments with reflectance of 0.51 Ro_{org}% , 0.57 Ro_{org}% and 0.57 Ro_{org}% (samples 17.1, 17.3 and 18.1, respectively).

All the reflectance values of organoclasts have been converted in Roeq%, considering the three equations mentioned above. Results have been reported in Table 4 and commented in the Discussion section.

5.4 PDI

The main advantage of the PDI method is the analytic and quantitative approach that, differently than other qualitative methods such as CAI, TAI and AAI, doesn't strictly depend on the operator's perception of colour and consequently is not empirical. Furthermore, the estimation of thermal maturity based on optical investigation of microfossils as PDI is rather inexpensive.

In this study, only Tasmanites from two samples (i.e. 4.4 and 5.3 Wenlock and Llandovery in age) were considered for PDI analysis (Fig. 9) because the other processed samples resulted barren in terms of palynomorphs content. PDI Tasmanites values were plotted on the diagram of Goodhue and Clayton (2010) suggesting a paleotemperature of about 130-135 °C. Although applied only to two samples, a cross check of the validity of this result, is provided by the corresponding Ro% value (about 0.9) indicating a middle-late mature stage for HC generation.

5.5 Raman analyses on Kerogen

Figure 10 show two representative spectra, before and after processing, for samples from the Łisogory region (Fig. 10 a-b) and from the Kielce region (Fig. 10 c-d). At a first glance, we can observe from the raw spectra collected (Fig. 10 a-c) significant differences in samples from the two blocks. First of all it is noteworthy the high fluorescence that affected samples from the Kielce block (Fig. 10 c) that is totally absent in Fig. 10 a.

High fluorescence background, is common in disordered carbonaceous materials that still contains aliphatic chains attached to the aromatic skeleton. This is already an indication of the degree of maturation of the organic matter, as fluorescence characterises thermal maturity stages with Ro values lower than 2, according to Quirico et al. (2005).

We refer to two different approaches for the two regions because samples pertain to different maturity level and spectra can be fitted only using different decomposition patterns and compared with different parametrizations.

In detail, all spectra from the Łysogory region were processes according to the analytical procedure described by Beyssac et al. (2002, 2003) and Lahfid et al. (2010) and paleotemperature were carried out from the parametrization of the RA1 and RA2 parameters. Results indicate that RA1 average value is 0.59 with a standard deviation of 0.009, while RA2 average value is 1.44 with a standard deviation of 0.053 (Table 5). Conversion into paleotemperatures provides mean values of 268.5 and 260.8°C (from RA1 and RA2 parameters, respectively) with a standard deviation of about 11°C for both parametrization (Table 5 and Fig. 10).

Spectra from samples collected in the Kielce region needed the subtraction of the baseline in order to avoid errors caused by high fluorescence. A third order polynomial baseline was applied as it better fitted the shape of all spectra. We found that the best solution for curve fitting was a mixed Gaussian-Lorentzian six bands deconvolution, in agreement with the works by Guedes et al. (2010; 2012) and Schito et al. (2016), performed on both bulk kerogen and single macerals (Fig. 10).

The width ratio between the D and G band (wD/wG) was also calculated using the new approach proposed by Schito et al. (2016). The authors suggested that the wD/wG parameter can be successfully used as it shows the best correlation against vitrinite reflectance on a set of samples of different ages, from lower Paleozoic to Cenozoic, and in a wide rangeof thermal maturity. As shown in Table 5, wD/wG values of the HCM samples have a mean value of 1.60 with a standard deviation of 0.049.

A further parameter, the distance between the D and G band position, has been used following the work of Liu et al. (2012). This parameter shows an average value of 238.55 cm^{-1} with a standard deviation of 6.45 cm^{-1} (Table 5).

5.6 Burial and Thermal modelling

Simplified reconstruction of the burial and thermal evolution of the Kielce block has been calibrated against organoclasts reflectance, I% in mixed layers I-S and Tmax data from the Llandovey to Ludlovian successions of the Bardo syncline (Fig. 11 a-b).

The burial history of this pseudowell, started in a deep water marine environment, with the deposition of 250m thick Ordovician shales, at about 488 My. During the Silurian deep water sedimentation went on with the deposition of Landovery to Lower Lludlow black shales and evolved to greywackes that represent the sedimentary infill of the Caledonian foreland basin since Lower Ludlovian times (Kozlowski et al., 2014). At that time, we observed a significant increase in sedimentation rate that passes from 0.08 to 0.25 mm/y. Then, the Pridolian was a period of scarce or null sedimentation as recognized by several authors (Kozlowski, 2008: Kozlowski et al., 2014, Gągała et al., 2015).

Sedimentation started again in Devonian times with shallow water sedimentation of sandstones during Lower Emsian that evolved in a carbonate deposition during the Lower/Middle Devonian boundary due to sea level rise (Szulczewski, 1996). The carbonate platform drowning (Szulczewski et al, 1996) occurred at the beginning of the Givetian and led to the deposition of about 700m thick black shales during the Upper Devonian and about 400m thick shales during the Lower Carboniferous.

An uplift event affected the Kielce region since 310My as indicated by the unconformity between the Upper Carboniferous and the Permian successions.

Sedimentation started again in the Upper Permian and continued during Triassic times with the deposition of continental and shallow marine sandstones and during Jurassic and Cretaceous times with the deposition of about 1400m thick limestones and marls. Maximum burial was achieved during this time were the base of Ordovician successions was buried at about 6000 m of depth.

A new uplift event took place at 70 My and was related to the regional uplift of the Mid Polish Trough (Dadlez, 1994) and led the erosion of about 3500m of rocks with an erosion rate of about 0.22 mm/yr.

The described evolution allows an acceptable calibration against organic and inorganic thermal indicators, as shown by the present-day maturity curve of Fig. 11 b.

To calibrate the thermal model of the Lysogory region we used thermal indicators and thicknesses values from the Silurian and Devonian successions that crop out in the Bodzentyn syncline. The evolutionary burial history of the Lysogory region is very similar to that previously described for the Kielce region until the upper Silurian (Fig. 12 a). The first difference can be found at the end of Lludlovian when the sedimentation continue, unlike in the Kielce block, with the deposition of basinal shales, marls and sandstones during all the Upper Silurian and went on during Lochkovian and Pragian ages.

The Lower/Middle Devonian carbonate platform shows higher thicknesses than those observed in the Kielce region, as well as the basin shales and marls deposits of the Upper Devonian that have a maximum thickness of about 2250m.

The Mesozoic phase of burial is significantly deeper than that recorded by the Kielce region and is characterized by 1200m thick Upper Permian and Triassic sandstones, 1500m thick Jurassic limestones and 1516m thick Cretaceous limestones and sandstones. This phase of burial led the base of the Ordovician successions at about 9000m of depth and the subsequent uplift eroded approximately 4.330m of rocks with an erosion rate of 0.26 mm/yr.

Calibration of this model is shown in Figure 12b showing a good fit for the Devonian and Upper Silurian reflectance values and I% in mixed layers I-S data. In addition, Figure 13 shows the evolution of thermal maturity through time attained by the base of Jurassic successions that fall between the immature stage and the early mature stages of HC generation according to our vitrinite reflectance and mineralogical data (R_o% of Hettangian samples between 0.51 and 0.57, Table 4).

5.8 2D distribution of thermal maturity data (old and new datasets)

Interpolation maps showing the distribution of thermal maturity parameters, expressed as HC generation windows in Cambrian-Ordovician, Silurian and Devonian intervals are reported in figure 13.

Interpolation was performed joining both literature and original data, except for Cambrian-Ordovician successions where new data in the Kielce block are not comparable with those from previous works. As shown in Figure 14 a mismatch arises when we compare literature and new data. Our results from analyses of the organic matter in Cambrian and Ordovician successions in the Kielce region, indicate a thermal maturity related to upper part of the oil window ($1 < Ro\% < 1.3$), while CAI data from Narkiewicz, (2002) mainly indicate mainly the early mature stages of HC generation ($1 < CAI < 2$). As a consequence it was not possible to obtain a comprehensive interpolation map using both datasets for this time interval. In addition, the poor spatial distribution of the new data did not allow us to build up an interpolation map that could stand alone. Thus we plotted thermal maturity derived from new data on the interpolation map obtained using literature data to highlight the discrepancies between the two.

Nevertheless, Cambrian data in the the Łisogory region carried out from Raman analyses on dispersed organi matter are consistent with CAI data (higher than 3), indicating the overmature stage of HC generation.

Moreover, it was possible to obtained two maps of distribution of thermal maturity for Silurian and Devonian successions using the whole set of reflectance data collected from previous works and from this study.

The map in Fig. 14 b shows that thermal maturity for Silurian successions in the Kielce block range between the early mature and the late mature stages of HC generation with a general increase from the South to the North. In the the Łisogory region data suggest a higher thermal maturity that mainly drops into the gas generation window.

Devonian successions experienced maturity in the early and mid-mature stage of HC generation in the Kielce block except for a restricted area located to the North East, near the HCF, where higher values of R_o% were collected. In the northern block, the scarceness and distribution of thermal maturity data did not allow a reliable interpolation. Nevertheless thermal maturity in the northern block, ranges between the mid and late mature stage of HC generation.

6 Discussion

6.1 Thermal maturity of Paleozoic succession

6.1.1 Ordovician to Devonian successions

Paleozoic rocks, in particular Silurian rocks, are major gas and oil source rocks in a wide range of geological contexts (Hasany and Khan, 2003). However, the assessment of thermal maturity for lower Paleozoic rocks by means of vitrinite reflectance is limited due to the lack of organic fragments derived from the degradation of the lignin-cellulose part of upper plants.

The use of organoclasts reflectance for Paleozoic rocks revealed to be a successfully alternative (Poprawa 2010, Petersen et al. 2013, Smolarek et al., 2014, Suárez-Ruiz et al. 2012). Neverthless, up to now, several equations that convert grapolites measurements into vitrinite-like reflectance values have been provided (Xianming et al., 2000; Petersen et al. 2013, Schmidt et al., 2015; Smolarek et al., 2014) but they lead to a range of levels of HC generation (Tab. 4). For this reason, we coupled organic matter optical analyses with Pyrolysis Rock Eval data, Raman spectroscopy performed on kerogen and X-ray diffraction of clay minerals, in order to correlate different thermal maturity indicators against different conversion for Paleozoic OM reflectance.

Graptolite and vitrinite-like reflectance values were calculated using three different formulas (Xianming et al., 2000; Petersen et al. 2013, Schmidt et al., 2015). As shown in table 4, vitrinite reflectance equivalent values differ significantly. In particular, formulas by Xianming et al. (2000) and Schmidt et al. (2015) provide values that are too high when compared with I% in mixed layers I-S and Tmax values. On the other hand, vitrinite reflectance equivalent values from Petersen et al.'s (2013) formula, indicate the early to mid mature stage of HC generation (Ro% between 0.66 and 0.92% for Silurian samples) that are consistent with Tmax data (between 437 and 442) and I% in mixed layers I-S (between 77 and 83) for samples collected at the Bardo syncline in the Kielce region (Table 1). In the Lysogory block, using the same formula, vitrinite reflectance equivalent values between 1.28 and 1.34 correspond to higher I% in mixed layers I-S that are proper of the first stage of gas generation.

Based on these assumptions, we applied Petersen et al. (2013)'s equation to convert organoclasts reflectance data into vitrinite reflectance equivalent data.

Obtained thermal maturity data indicate a marked difference in thermal maturity of Ordovician to Devonian samples, between the Łysogory and Kielce blocks, in agreement with previous works (Marynowski et al., 2001; Narkiewicz, 2002; Rospondek et al., 2008; Smolarek et al., 2014; Szczepanik, 1997, 2001). In detail data distribution traces an abrupt jump between the thermal maturity of the Kielce and the Łisogory blocks composing the HCM structure, from the early-late mature to mid mature-overmature, respectively.

Nevertheless, these differences cannot be appreciated in the Devonian samples in the northwestern sector of the Kielce block, where Tmax, R_{oeq}% and I% in I-S data display higher levels of thermal maturity. These data indicate higher maturities than those found by Rospondek et al. (2008), Marynowski et al. (2001) and Narkiewicz et al. (2002) which are anyway unusually higher than the rest of the Kielce block. According to Narkiewicz et al. (2002) this area is a part of the Łysogory block rather than the Kielce. Field evidences in the Mogiłki quarry near Kielce revealed an intense tectonics characterized by giant reverse folds and thrusts that can be the cause of this thermal maturity anomaly. Thrusting related to the Holy Cross Fault movement probably in the latest Silurian-earliest Devonian (Late Caledonian deformation, Gągała et al., 2015) would have produced a tectonic loading which affected thermal maturity. This evidence is strengthened by the repeated strata in the stratigraphy of the Piekosow 1 well (Fig. 2b).

6.1.2 Cambrian succession

Data for the Cambrian successions show that: 1) samples experienced paleotemperatures consistent with anchizone conditions as confirmed by the presence pirophyllite in the <2 μm grain size fraction and by Raman analyses on dispersed organic matter that display paleotemperatures between 260 and 268°C in the northern region; 2) lower levels of thermal maturity in deep diagenetic conditions as indicated by o vitrinite reflectance (1.03%) and mixed layers I-S (R1-R3 structures) data were found in the Kielce block.Raman parameters carried out on sample 7.1 in the Kielce region, doesn't provide a straightforward solution in terms of paleotemperatures or levels of thermal maturity because an univocal parametrization between Raman parameters and thermal maturity in diagenesis has not yet been defined. Nevertheless, we can compare our results with those derived on kerogen at similar thermal maturity levels (Liu et al., 2012; Schito et al., 2016). In Figure 15 a are plotted wD/wG ratio parameters against Ro% obtained from Raman analyses by Schito et al. (2016) and in Figure 15 b are plotted values of the distance between D and G peaks from Liu et al. (2012) obtained on different samples (bitumen, coal with different ranks and graptolites). The same parameters calculated for our samples are plotted on the y axes and are represented by the light grey rectangle, whose thickness is proportionated to the standard deviation. As we can see from the figure, Raman data in this work correspond to previous data that show vitrinite reflectance values of about 1-1.3% (Fig. 15 a) or between 1 and 1.5% (Fig. 15 b).

Therefore, even if Raman parameters on Cambrian rocks cannot be precisely correlated to vitrinite reflectance, they suggest a thermal maturity typical of the upper portion of the oil window and initial gas generation (about 1-1.5 R_o%). This evidence is also in agreement with results provided by the thermal model performed in the Bardo syncline, according to which the base of the Ordovician interval entered in the upper part of the oil window during the Mesozoic phase of maximum burial.

6.2 Thermal modelling

The main points to be analysed when discussing a burial and thermal model are: 1) the reliability of thermal maturity indicators; 2) the thickness of the stratigraphic intervals used to build up the pseudo-wells; 3) the variation in the heat-flow through time in the studied area.

Concerning the first point, we have already discussed this topic in the previous paragraph.

Concerning succession thickness used to simulate burial history of the two pseudo-wells, they are in agreement with previous works (Gągała, 2015; Kozlowski, 2008; Narkiewicz, 2002) and are constrained by present day thicknesses measured in several wells. On the other hand, the amount of burial related to the Late phases of Variscan orogenesis is still poorly constrained and needs to be further discussed. In the Kielce region the amount of sediments deposited during the Lower Carboniferous is constrained by measures in the well Galezice G-5 located a few kilometres to the west of Kielce town (Fig. 2b), while the same stratigraphic interval was totally eroded in the Łysogory block. Lower Carboniferous thicknesses can be found only in one well further to the north (Ostalow PIG-2 Fig. 2b) and they are of about 400 m.

Kutek and Głazek (1972) and Narkeiwicz (2010) suggest that thermal maturity of the Paleozoic successions could have been taken place during Late Paleozoic (Late Carbonifeours-Early Permian). Nevertheless, our simulation of maturation as a response of a Upper Paleozoic burial in the Łysogory region would have implied an amount of about 6 km of sediments that is difficult to explain during a period characterised by compressional tectonic, at least since Late Carboniferous times (Lamarche et al, 2002; 2003). Indeed, Narkiewicz et al. (2002; 2010) proposed an increase of heat flow values at the end of Paleozoic to justify its burial model, but this hypothesis is not consistent with our data for two reasons:

1) the thermal maturity curve fits Silurian thermal indicators from the Kielce region only with a heat flow values of 35 mW/m^2 during the Carboniferous, much lower than the present day one of about 45 W/m^2 if we use present day thicknesses of both Paleozoic and Mesozoic successions;
2) the high slope of the maturity curve for Devonian and Silurian data (Fig. 11 b) can be traced only with an Mesozoic burial of about 4000m rather than with an increase of heat flow values in the Lysogory block.

In conclusion, the burial history proposed in this work, shows a very similar evolution for the two tectonic blocks in the HCM, except for the sediments thicknesses that are always higher in the Łysogory region, both in Paleozoic and Mesozoic times. This can be the result of the Holy Cross Fault poli-phase tectonic activity with either normal or reverse motions with scarse to null strike-slip components. This interpretation is in good agreement with a recent work by Schätz et al. (2006) that, on the base of paleomagnetic data, suggests that no large scale tectonic horizontal translation were recognized after Middle Ordovician times, but is in contrast with the hypothesis of Narkiewicz (2002) and Dadlez (1994) that considered the two blocks as separated from Cambrian to Devonian and then welded together as a result of movements along the TTZ of the Malopolska block during late Pragian-early Emsian times.

6.3 Timing of HC generation and source rock evaluation

Thermal maturity indicators derived from the organic and inorganic fraction of sediments indicate differences in thermal maturity for the Paleozoic successions exposed in the Kielce and Łysogory blocks, and suggest for HC exploration thermal maturities associated with gas generation in the Łysogory block and with oil generation in the Kielce block, except for its north-western sector.

What is important to stress, in view of the exploration of Paleozoic source rocks, is the timing of HC generation, whose effect is crucial in the evaluation of the organic matter conversion rate (Gretener and Curtis, 1982) and to model the migration of HC resources during the geological evolution of a basin.

Both our thermal models presented in this paper indicate that maximum burial was attained in the two blocks about 70 My ago, almost at the end of Mesozoic times. Nevertheless our models indicate that the Ordovician to Upper Silurian successions entered in the early mature stage of the oil window between 390 and 360 My in the Kielce region, and between 390 and 380 My in the Łysogory block. The Ordovician section of the Kielce block entered the oil window mid-mature stage between 320 and 300My, while Ordovician, Lower Silurian and the lower part of the Upper Silurian section in the Łysogory block experienced the same maturation between 370 and 350 My ago (Figs 11 a and 12 a). Furthermore, Ordovician to Upper Silurian successions in the Łysogory block entered in the upper portion of the oil window at 220 to 180 My and experienced the gas generation in a time that span between 160 and 70My (Fig. 12 a).

According to our model, Lower Devonian successions entered in the oil window 160 My ago in the Kielce region, while,in the Łysogory block the bottom of Lower Devonian strata entered in the oil window at about 360My, in the mid mature stage of oil generation at about 200My and only at 130My entered the upper portion of oil window (Figs. 11 a and 12 a).

Coupling our results from thermal models and 2D distribution of thermal maturity for Silurian and Devonian rocks, with results obtained from Pyrolysis Rock-Eval, we can assess the source rocks with the highest potential in the area are the Silurian shales of the Bardo syncline samples and the Middle Devonian samples from the Gruchawaka area (sample 16.2; Fig. 6) for oil generation in the Kielce block, while only Jurassic samples indicate good source rocks for oil generation moving toward the northern block.

6 Conclusions

In this paper, we successfully face thermal maturity and source rocks assessment issues of a complicate Paleozoic area devoid of vitrinite macerals and reconstructed two reliable thermal history models for the Holy Cross Mountains which were affected by poliphasic events of subsidence and uplift.

In detail, we obtained different main results:

1) Organoclasts reflectance measured by optical analysis should be converted into vitrinite reflectance equivalent values by Petersen et al., (2013)'s equation as data are consistent with other thermal maturity indicators carried out from Pyrolysis Rock Eval and X-ray diffraction of clay minerals;
2) Two new promising tools for thermal maturity assessment for Lower Paleozoic rocks that are Raman spectroscopy and PDI to be used on Paleozoic palynofacies have been proposed;
3) Pyrolysis Rock Eval and TOC analyses indicate that the most productive source rocks in the the Holy Cross Mountains are the Silurian and Ordovician black shales cropping out in the Bardo syncline of the Kielce block;
4) We drew a series of maps including published and original thermal maturity data in order to provide a comprehensive datasets to be used for hydrocarbon exploration;
5) Thermal models outlined differences in terms of burial during the Silurian-Devonian interval and in Mesozoic times for the Lysogory and Kielce blocks. These differences are mainly due to the reactivation of the Holy Cross Fault as a normal fault the led to the accumulation of large amounts of sediments in the Lysogory block.

Acknowledgement

We are greatly indebted with ENI GEBA and ENI Labs for sponsoring field work and providing pyrolisis facilieties. Stefano Mazzoli, Massimiliano Zattin, Benedetta Andreucci, Ada Castelluccio, Leszek Jankowski and Rafal Szaniawski are warmly acknowledged for passionate discussions on Polish geology and support in sampling phases. Thanks to Stefano Celano for the preliminary organisation of the dataset of existing thermal maturity data. Jan Golonka kindly contributed to discussions on Holy Cross Mts tectonic evolution. Palynological slides are stored at the Sedimentary Organic Matter Laboratory of the Department of Physics and Geology (University of Perugia, Italy) and Reflectance specimen at the Academic Laboratory of Basin Analysis of the Department of Science Roma Tre University, Italy) Fundings: MIUR grants to Roma Tre PhD School in Earth Sciences (XXVIII doctoral cycle).

References

Aldega, L., Corrado, S., Grasso, M., and Maniscalco, R., 2007, Correlation of diagenetic data from organic and inorganic studies in the Apenninic Maghrebian fold and thrust belt: a case study from Eastern Sicily: The Journal of Geology, v. 115, no. 3, p. 335-353.

Aldega, L., Corrado, S., Carminati, E., Shaban, A., and Sherkati S., 2014. Thermal evolution of the Kuh-e-Asmari and Sim anticlines in the Zagros fold-and-thrust belt: implications for hydrocarbon generation. Marine and Petroleum Geology, 57, 1-13.

ASTM D7708-14, Standard Test Method for Microscopical Determination of the Reflectance of Vitrinite Dispersed in Sedimentary Rocks, ASTM International, West Conshohocken, PA, 2014, www.astm.org

Basin Mod. 1-D for WindowsTM, 1996." A Basin Analysis Modelling System version 5: 386.

Belka, Z., 1990, Thermal maturation and burial history from conodont colour alteration data, Holy Cross Mountains, Poland: Courier Forschungsinstitut Senckenberg, v. 118, p. 241-251.

Bertrand, R., and Heroux, Y., 1987, Chitinozoan, graptolite, and scolecodont reflectance as an alternative to vitrinite and pyrobitumen reflectance in Ordovician and Silurian strata, Anticosti Island, Quebec, Canada: AAPG Bulletin, v. 71, no. 8, p. 951-957.

Bertrand, R., 1990, Correlations among the reflectances of vitrinite, chitinozoans, graptolites and scolecodonts: Organic Geochemistry, v. 15, no. 6, p. 565-574.

Beyssac, O., Goffé, B., Chopin, C., and Rouzaud, J., 2002, Raman spectra of carbonaceous material in metasediments: a new geothermometer: Journal of metamorphic Geology, v. 20, no. 9, p. 859-871.

Bertrand, R., & Malo, M. (2012). Dispersed organic matter reflectance and thermal maturation in four hydrocarbon exploration wells in the Hudson Bay Basin: regional implications. Geological Survey of Canada, Open File, 7066, 54.

Beyssac, O., Goffé, B., Petitet, J.-P., Froigneux, E., Moreau, M., and Rouzaud, J.-N., 2003, On the characterization of disordered and heterogeneous carbonaceous materials by Raman spectroscopy: Spectrochimica Acta Part A: Molecular and Biomolecular Spectroscopy, v. 59, no. 10, p. 2267-2276.

Burnham, A. K., & Sweeney, J. J. (1989). A chemical kinetic model of vitrinite maturation and reflectance. Geochimica et Cosmochimica Acta, 53(10), 2649-2657.

Bustin, R., Link, C., and Goodarzi, F., 1989, Optical properties and chemistry of graptolite periderm following laboratory simulated maturation: Organic geochemistry, v. 14, no. 4, p. 355-364.

Butler, R. W., 1991, Hydrocarbon maturation, migration and tectonic loading in the Western Alpine foreland thrust belt: Geological Society, London, Special Publications, v. 59, no. 1, p. 227-244.

Caricchi, C., Corrado S., Di Paolo, L., Aldega, L. and Grigo D., 2016. Thermal maturity of Silurian deposits in the Baltic Syneclise (on-shore Polish Baltic Basin): contribution to unconventional resources assessment. Ital. J. Geosci., Vol. 135, No. 3, pp. 000-000, 5 figs., 4 tabs. DOI:10.3301/IJG.2015.16

Carlini M., Artoni A., Aldega L., Balestrieri M.L., Corrado, S., Vescovi P., Bernini M., & Torelli L. (2013). Exhumation and reshaping of far-travelled/allochthonous tectonic units in mountain belts. New insights for the relationships between shortening and coeval extension in the western Northern Apennines (Italy). Tectonophysics, 608,267–287.

Corrado S., Aldega L., Balestrieri, M.L., Maniscalco R. & Grasso M. (2009) - Structural evolution of the sedimetary accretionary wedge of the alpine system in Eastern Sicily: thermal and thermochronological constraints. Geological Society of America Bulletin, 121, 1475-1490.

Dadlez, R., Kowalczewski, Z., and Znosko, J., 1994, Some key problems of the pre-Permian tectonics of Poland: Geological Quarterly, v. 38, no. 2, p. 169-190.

Dadlez, R., 2001, Holy Cross Mts. area—crustal structure, geophysical data and general geology: Geological Quarterly, v. 45, no. 2, p. 99–106.

Dubessy, J., Caumon, M. C., & Rull, F. (Eds.). (2012). Raman spectroscopy applied to earth sciences and cultural heritage (Vol. 12). The Mineralogical Society of Great Britain and Ireland.

Ferrari, a., and Robertson, J., 2000, Interpretation of Raman spectra of disordered and amorphous carbon: Physical Review B, v. 61, no. 20, p. 14095-14107.

Ferrari, A. C., and Robertson, J., 2004, Raman spectroscopy of amorphous, nanostructured, diamond–like carbon, and nanodiamond: Philosophical Transactions of the Royal Society of London A: Mathematical, Physical and Engineering Sciences, v. 362, no. 1824, p. 2477-2512.

Gągała, L., 2015, Late Silurian deformation in the Łysogóry Region of the Holy Cross Mountains revisited: restoration of a progressive Caledonian unconformity in the Klonów Anticline and its implications for the kinematics of the Holy Cross Fault (Central Poland): Geological Quarterly, v. 58, no. 1, p. 10.7306/gq. 1222.

Giampaolo, C., and Lo Mastro, S., 2000, Analisi (semi) quantitativa delle argille mediante diffrazione a raggi x: Incontri Scientifici, v. 2, p. 109-146.

Goodarzi, F., and Norford, B., 1987, Optical properties of graptolite epiderm—a review: Bull. Geol. Soc. Denmark, v. 35, p. 141-147.

Goodarzi, F., and Norford, B., 1989, Variation of graptolite reflectance with depth of burial: International journal of coal geology, v. 11, no. 2, p. 127-141.

Goodhue, R., & Clayton, G. (2010). Palynomorph Darkness Index (PDI)–a new technique for assessing thermal maturity. Palynology.

Gretener, P. E., & Curtis, C. D. (1982). Role of Temperature and Time on Organic Metamorphism: GEOLOGIC NOTES. AAPG Bulletin, 66(8), 1124-1129.

Guedes, A., Valentim, B., Prieto, A. C., Rodrigues, S., and Noronha, F., 2010, Micro-Raman spectroscopy of collotelinite, fusinite and macrinite: International Journal of Coal Geology, v. 83, no. 4, p. 415-422.

Guedes, A., Valentim, B., Prieto, A., and Noronha, F., 2012, Raman spectroscopy of coal macerals and fluidized bed char morphotypes: Fuel, v. 97, p. 443-449.

Hackley, P. C., & Cardott, B. J. (2016). Application of organic petrography in North American shale petroleum systems: A review. International Journal of Coal Geology, 163, 8-51.

Hasany, S. T., and Khan, F.-i.-R., 2003, Palaeozoic sequences as potential source rocks for petroleum in northwestern pakistan, with particular refrence to the silurian system, a major petroleum source in the middle east and north Africa Pakistan Association of Petroleum Geoscientists PAPG/SPE ANNUAL TECHNICAL CONFERENCE 2003. Best Practices & New Technologies, October 3-5, 2003, Islamabad, Pakistan.

Hoffman, J., 1979, Clay mineral assemblages as low grade metamorphic geothermometers: application to the thrust faulted disturbed belt of Montana, USA.

Jäger, H. 2016, Optical Kerogen Analysis for enhanced analysis of hydrocarbon systems: From mature European basins to new exploration in northern Gondwana. ICPSG – INTERNATIONAL CONGRESS ON "PALAEOZOIC STRATIGRAPHY OF GONDWANA" April 14-16, 2016 – Perugia, Italy.

Jagodzinski, H., 1949, Eindimensionale Fehlordnung in Kristallen und ihr Einfluss auf die Röntgeninterferenzen. I. Berechnung des Fehlordnungsgrades aus den Röntgenintensitäten: Acta crystallographica, v. 2, no. 4, p. 201-207.

Jaworowski, K., and Sikorska, M., 2006, Łysogóry Unit (Central Poland) versus East European Craton--application of sedimentological data from Cambrian siliciclastic association: Geological Quarterly, v. 50, no. 1, p. 77-88.

Konon, A., 2004, Successive episodes of normal faulting and fracturing resulting from progressive extension during the uplift of the Holy Cross Mountains, Poland: Journal of structural geology, v. 26, no. 3, p. 419-433.

Konon, A., 2007, Strike-slip faulting in the Kielce Unit, Holy Cross Mountains, central Poland: Acta Geologica Polonica, v. 57, p. 415-441.

Kowalczewski, Z., 1974, Geological and structural aspects of magmatism in the Góry Świętokrzyskie Mts. Against the back-ground of recent research (in Polish with English summary): Biul. Inst. Geol, v. 275, p. 11-62.

Kozłowski, W., 2008, Lithostratigraphy and regional significance of the Nowa Słupia Group (Upper Silurian) of the Łysogóry Region (Holy Cross Mountains, Central Poland): Acta Geologica Polonica, v. 58, no. 1, p. 43-74.

Kozłowski, W., Domańska-Siuda, J., and Nawrocki, J., 2014, Geochemistry and petrology of the Upper Silurian greywackes from the Holy Cross Mountains (central Poland): implications for the Caledonian history of the southern part of the Trans-European Suture Zone (TESZ): Geological Quarterly, v. 58, no. 2, p. 311-336; doi: 310.7306/gq. 1160.

Kutek, J., and Głazek, J., 1972, The Holy Cross area, central Poland, in the Alpine cycle: Acta Geologica Polonica, v. 22, no. 4, p. 603-651.

Kutek, J., 2001, The Polish Permo-Mesozoic Rift Basin: Mémoires du Muséum national d'histoire naturelle, v. 186, p. 213-236.

Lahfid, A., Beyssac, O., Deville, E., Negro, F., Chopin, C., and Goffé, B., 2010, Evolution of the Raman spectrum of carbonaceous material in low-grade metasediments of the Glarus Alps (Switzerland): Terra Nova, v. 22, no. 5, p. 354-360.

Lamarche, J., Mansy, J., Bergerat, F., Averbuch, O., Hakenberg, M., Lewandowski, M., Stupnicka, E., Swidrowska, J., Wajsprych, B., and Wieczorek, J., 1999, Variscan tectonics in the Holy Cross Mountains (Poland) and the role of structural inheritance during Alpine tectonics: Tectonophysics, v. 313, no. 1, p. 171-186.

Lamarche, J., Bergerat, F., Lewandowski, M., Mansy, J. L., Świdrowska, J., & Wieczorek, J. (2002). Variscan to Alpine heterogeneous palaeo-stress field above a major Palaeozoic suture in the Carpathian foreland (southeastern Poland). Tectonophysics, 357(1), 55-80.

Lamarche, J., Lewandowski, M., Mansy, J. L., & Szulczewski, M. (2003). Partitioning pre-, syn-and post-Variscan deformation in the Holy Cross Mountains, eastern Variscan foreland. Geological Society, London, Special Publications, 208(1), 159-184.

Langford, F., and Blanc-Valleron, M.-M., 1990, Interpreting Rock-Eval Pyrolysis Data Using Graphs of Pyrolizable Hydrocarbons vs. Total Organic Carbon (1): AAPG Bulletin, v. 74, no. 6, p. 799-804.

Li, C.-Z., 2007, Some recent advances in the understanding of the pyrolysis and gasification behaviour of Victorian brown coal: Fuel, v. 86, no. 12, p. 1664-1683.

Liu, D., Xiao, X., Tian, H., Min, Y., Zhou, Q., Cheng, P., and Shen, J., 2012, Sample maturation calculated using Raman spectroscopic parameters for solid organics: Methodology and geological applications: Chinese Science Bulletin, v. 58, no. 11, p. 1285-1298.

Malec, J., Więcław, D., and Zbroja, S., 2010, The preliminary assessment of the selected Paleozoic deposits of the Holy Cross Mountains: Geology, Geophysics and Environment, v. 36, no. 1, p. 5.

Marynowski, L., Czechowski, F., and Simoneit, B. R., 2001, Phenylnaphthalenes and polyphenyls in Palaeozoic source rocks of the Holy Cross Mountains, Poland: Organic Geochemistry, v. 32, no. 1, p. 69-85.

Meneghini, F., Botti, F., Aldega, L., Boschi, C., Corrado, S., Marroni, M., and Pandolfi, L., 2012, Hot fluid pumping along shallow-level collisional thrusts: the Monte Rentella Shear Zone, Umbria Apennine, Italy: Journal of Structural Geology, v. 37, p. 36-52.

Merriman, R., and Frey, M., 1999, Patterns of very low-grade metamorphism in metapelitic rocks: Low-grade metamorphism, p. 61-107.

Mizerski, W., 2004, Holy Cross Mountains in the Caledonian, Variscan and Alpine cycles–major problems, open questions: Prz. Geol, v. 52, no. 8/2, p. 774-779.

Moore, D. M., and Reynolds, R. C., 1989, X-ray Diffraction and the Identification and Analysis of Clay Minerals, Oxford university press Oxford.

Moore, D. M., & Reynolds Jr, R. C. (1997) X-ray Diffraction and the Identification and Analysis of Clay Minerals.

Mustafa, K. A., Sephton, M. A., Watson, J. S., Spathopoulos, F., and Krzywiec, P., 2015, Organic geochemical characteristics of black shales across the Ordovician–Silurian boundary in the Holy Cross Mountains, central Poland: Marine and Petroleum Geology, v. 66, p. 1042-1055.

Narkiewicz, M., 2002, Ordovician through earliest Devonian development of the Holy Cross Mts.(Poland): constraints from subsidence analysis and thermal maturity data: Geological Quarterly, v. 46, no. 3, p. 255-266.

Narkiewicz, K., and Narkiewicz, M., 2010, Mid Devonian carbonate platform development in the Holy Cross Mts. area (central Poland): new constraints from the conodont Bipennatus fauna: Neues Jahrbuch für Geologie und Paläontologie-Abhandlungen, v. 255, no. 3, p. 287-300.

Nöth, S., Karg, H., and Littke, R., 2001, Reconstruction of Late Paleozoic heat flows and burial histories at the Rhenohercynian-Subvariscan boundary, Germany: International Journal of Earth Sciences, v. 90, no. 2, p. 234-256.

Oncken, O., 1982, The reconstruction or the geosyncline history with the help of coalification gradients (as for example, the Ebbe anticline in the Rhein Slate Mountains): Geologische Rundschau, v. 71, no. 2, p. 579-602.

Petersen, H.I., Schovsbo, N.H., & Nielsen, A.T. (2013). Reflectance measurements of zooclasts and solid bitumen in Lower Paleozoic shales, southern Scandinavia: Correlation to vitrinite reflectance. International Journal of Coal Geology, 114, 1-18. DOI: 10.1016/j.coal.2013.03.013.

Pollastro, R. M. (1990). The illite/smectite geothermometer—concepts, methodology, and application to basin history and hydrocarbon generation. Rocky Mountain Section (SEPM).

Poprawa, P., Żywiecki, M., and Grotek, I., 2005, Burial and thermal history of the Holy Cross Mts. area-preliminary results of maturity modelling: Polskie Towarzystwo Mineralogiczne, v. 26, p. 251-254.

Poprawa, P., Kosakowski, P., & Wróbel, M. (2010). Burial and thermal history of the Polish part of the Baltic region.Geological Quarterly, 54(2), 131-142.

Quirico, E., Rouzaud, J. N., Bonal, L., and Montagnac, G., 2005, Maturation grade of coals as revealed by Raman spectroscopy: progress and problems: Spectrochim Acta A Mol Biomol Spectrosc, v. 61, no. 10, p. 2368-2377.

Rospondek, M., Szczerba, M., Malek, K., Góra, M., and Marynowski, L., 2008, Comparison of phenyldibenzothiophene distributions predicted from molecular modelling with relevant experimental and geological data: Organic Geochemistry, v. 39, no. 12, p. 1800-1815.

Sclater, J. G., and Christie, P., 1980, Continental stretching: An explanation of the post-mid-cretaceous subsidence of the central North Sea basin: Journal of Geophysical Research: Solid Earth (1978– 2012), v. 85, no. B7, p. 3711-3739.

Schätz, M., Zwing, A., Tait, J., Belka, Z., Soffel, H., and Bachtadse, V., 2006, Paleomagnetism of Ordovician carbonate rocks from Malopolska Massif, Holy Cross Mountains, SE Poland—

magnetostratigraphic and geotectonic implications: Earth and Planetary Science Letters, v. 244, no. 1, p. 349-360.

Schito, A., Corrado, S., Romano, C., Guedes, A., Grigo, D., New frontiers for the assessment of thermal maturity of kerogen: application of Raman spectroscopy to diagenesis. In European Regional Conference and Exhibition.AAPG, May 19th - 20th, 2016-Bucharest, Romania

Schmidt, J.S., Araujo, C.V., Souza, I.V.A.F. & Chakas, R.B.A. (2015). Hydrous pyrolysis maturation of vitrinite- like and humic vitrinite macerals: Implications for thermal maturity analysis. International Journal of Coal Geology, 144-145, 5-14. DOI: 10.1016/j.coal.2015.03.016.

Smolarek, J., Marynowski, L., Spunda, K., and Trela, W., 2014, Vitrinite equivalent reflectance of Silurian black shales from the Holy Cross Mountains, Poland: Mineralogia, v. 45, no. 3-4, p. 79-96.

Stach, E. (1982). Stach's textbook of coal petrology.

Suárez-Ruiz, I., Flores, D., Filho, J.G.M., & Hackley, P.C. (2012). Review and update of the applications of organic petrology: Part 1, geological applications. International Journal of Coal Geology, 99, 54-112. DOI: 10.1016/j.coal.2012.02.004.

Sweeney, J. J., and Burnham, A. K., 1990, Evaluation of a Simple Model of Vitrinite Reflectance Based on Chemical Kinetics (1): AAPG Bulletin, v. 74, no. 10, p. 1559-1570.

Szulczewski, M., Belka, Z., and Skompski, S., 1996, The drowning of a carbonate platform: an example from the Devonian-Carboniferous of the southwestern Holy Cross Mountains, Poland: Sedimentary Geology, v. 106, no. 1, p. 21-49.

Szczepanik, Z., 1997, Preliminary results of thermal alteration investigations of the Cambrian acritarchs in the Holy Cross Mts: Geological Quarterly, v. 41, no. 3, p. 257-264.

Szczepanik, Z., 2001, Acritarchs from Cam brian de pos its of the south ern part of the Łysogóry unit in the Holy Cross Moun tains, Poland.

Taylor, G. H., 1998, Organic petrology: A new handbook incorporating some revised parts of Stach's textbook of coal petrology, Gebruder Borntraeger Verlagsbuchhandlung.

Teichmüller, M. 1987. Organic material and very low grade metamorphism. In Frey, M., ed. Low-temperature metamorphism. Glasgow, Chapman & Hall, p. 114–161.

Tricker, P. M., Marshall, J. E., and Badman, T. D., 1992, Chitinozoan reflectance: a Lower Palaeozoic thermal maturity indicator: Marine and petroleum geology, v. 9, no. 3, p. 302-307.

Trela, W. (2007). Upper Ordovician mudrock facies and trace fossils in the northern Holy Cross Mountains, Poland, and their relation to oxygen-and sea-level dynamics. Palaeogeography, Palaeoclimatology, Palaeoecology, 246(2), 488-501.

Urban, J., and Gągal, J., 2008, Geological heritage of the Œwiêtokrzyskie (Holy Cross) Mountains (Central Poland).

Wilkins, R. W., Boudou, R., Sherwood, N., and Xiao, X., 2014, Thermal maturity evaluation from inertinites by Raman spectroscopy: The 'RaMM'technique: International Journal of Coal Geology, v. 128, p. 143-152.

Wopenka, B., and Pasteris, J. D., 1993, Structural characterization of kerogens to granulite-facies graphite: applicability of Raman microprobe spectroscopy: The American Mineralogist, v. 78, no. 5-6, p. 533-557.

Xianming, X., Wilkins, R.W.T., Dehan, L., Zufa, L., & Jiamu, F. (2000). Investigation of thermal maturity of Lower Palaeozoic hydrocarbon source rocks by means of vitrinite-like maceral reflectance – a Tarim Basin case study. Organic Geochemistry, 31(10), 1041-1052. DOI: 10.1016/S0146-6380(00)00061-9.

Figure Caption

Figure 1. Location of the study area (dashed square) and shale and oil prospectivity in Poland, http://www.ogj.com

Figure 2. (a) Geological map of the Paleozoic successions in the HCM with sampling location (modified and redrawn after Kononk, 2007); (b) simplified sketch of the Mesozoic cover in the HCM area showing sampling and wells location. Acronyms: HCF = Holy Cross Fault

Figure 3. Stratigraphy of the Paleozoic succession in the Łysogory (a) and Kielce blocks (b). Modified and redrawn after Kozlowski (2008) and Gągała (2015)

Figure 4. Distribution of thermal maturity indicators for Cambrian-Ordovician (a), Silurian (b) and Devonian (c) stratigraphic intervals compiled after Belka (1990); Marynowski et al. (2001); Narkiewicz (2002); Smolarek et al. (2014); Szczepanik (1997, 2001)

Figure 5. Distribution of organic and inorganic thermal maturity indicators (from this work) for Paleozoic (a) and Mesozoic (b) successions

Figure 6. S1+S2 pyrolysis data vs. total organic carbon diagram showing the petroleum source rock potential for Cambrian to Jurassic rocks

Figure 7. Microphotographs from polished section (sample 1.1) showing high reflectance values that vary between about 2 (a) and 12 (b)

Figure 8. Microphotograph of a graptolite at 50X in oil immersion

Figure 9. Four specimens of Tasmanites selected for PDI (1: slide 4.4, e.f. P38; 2: slide 4.4, e.f. T22/1; 3: slide 5.3, e.f. V28/3; slide 5.3., e.f. L24/2). Each specimen (5-8) shows 10 selected areas where PDI was determined after the grey scale conversion (for further details please see Goodhue and Clayton, 2010, p. 148)

Figure 10. Raman spectra of organic matter dispersed in Cambrian rocks. (a) Raw spectra for sample 1.1; (b) spectra deconvolution with a five-peaks fitting according to Lahfid et al., (2010). The figure shows the bands (D, D2, D3, D4, G) used to calculate RA1 and RA2 parameters; (c) raw spectra for sample 7.1; (d) spectra deconvolution after baseline subtraction fitting with a six-peaks deconvolution according to Guedes et al., (2010) and Schito et al., (2016). The figure shows the position of the D and G bands

Figure 11. (a) 1D burial and thermal history of the Paleozoic successions from the Kielce region; (b) heat flow distribution through time; (c) present-day maturity data for Silurian rocks calibrated against organic and inorganic thermal indicators

Figure 12. (a) 1D burial and thermal history of the Paleozoic successions from the Lysogory region; (b) heat flow distribution through time; (c) present-day maturity data for Silurian and Devonian rocks calibrated against organic and inorganic thermal indicators

Figure 13. Maturity evolution of the Jurassic succession in the Lysogory region. The lower line indicates the top of the Jurassic sediments, while the upper line indicates its bottom

Figure 14. (a) Thermal maturity map of Cambrian and Ordovician successions derived from published and original thermal maturity indicators . Data from Narkiewicz, (2002) and Szczepanik (1997; 2001) are shown by the dark squares. Original organoclasts reflectance data are indicated by the white dots, or by the white and dark triangles when performed by Raman spectroscopy. The question mark highlights the mismatch

between original and previous data in the Kielce Block (see text); (b) thermal maturity map of Silurian successions derived from original (white dots) and published data (Narkiewicz,2002; Smolarek et al., 2014; dark dots); (c) thermal maturity map of Devonian successions derived from original (white dots) and published data (Belka, 1990; Marynowski et al. 2001; Rospondek et al., 2008; dark dots).

Figure 15. (a) Comparison between our data and maturity trend provided by Schito et al., (2016) for the wD/wG values. Our data are indicated by the light grey area whose heigth represents the standard deviation; (b) comparison between our data and maturity trend provided by Liu et al., (2012) for the D-G distance values. Our data are indicated by the light grey area whose heigth represents the standard deviation. Acronyms: wD/wG = full width at maximum height ratio between the D and G band; D-G distance = difference between G band and D band position, in cm^{-1}

Table 1. Summary of details for sampling location (coordinates, ages, tectonic block and lithology).

Table 2. X–ray semiquantitative analysis of the whole rock composition and <2 μm grain size fraction for the Paleozoic to Jurassic succession. Acronyms: % I in I-S— illite content in mixed layers illite-smectite; R — stacking order of mixed layers I-S; % C in C-S— chlorite content in mixed layers chlorite-smectite; Sm – smectite; C-S - mixed layers chlorite-smectite; Rec - rectorite; I— illite; I-S - mixed-layers illite-smectite; Kln— kaolinite; Chl— chlorite; Qtz— quartz; Cal— calcite; Dol - dolomite; Kfs— K feldspar; Pl— plagioclase; Ph— phyllosilicates; Sid— siderite; Py— pyrite; Hem – hematite; Ank - ankerite; Gt - goethite; Prl – pyrophyllite; N.D. – not determined. Subscript numbers correspond to mineral weight percentages.

Table 3. Summary of pyrolysis Rock Eval data. Acronyms: TOC – total organic carbon; HI – hydrogen index; Tmax: temperature at which S2 reaches its maximum; S1 = measure of volatilization of free hydrocarbons during the first stage of heating; S2 = quantity of hydrocarbons released from thermal cracking during the second stage of heating; N.D. – not determined.

Table 4. Organoclasts and vitrinite reflectance data for the Paleozoic to Jurassic succession. Acronyms: Ro_{org}% - orgaoclasts reflectance; R_o%- vitrinite reflectance; R_{oeq}% - vitrinite reflectance equivalent values according to different authors; SD – standard deviation; N.D. – not determined; Nr. Meas. – number of measurements. 1 = conversion using Xianming et al., (2000) formula; 2 = conversion using Petersen et al., (2013) formula; 3 = conversion using Schmidt et al., (2015) formula.

Table 5. Mean Raman parameters obtained from the Upper Cambrian samples in the Łysogory Block (1.1 and 1.2) and from the Lower Cambrian sample in the Kielce Block (7.1). Acronyms: RA1 = (D + D4)⁄(D + D2 + D3 + D4 + G) area ratio; RA2 = (D + D4)⁄(D2 + D3 + G) area ratio; T°C (RA1) = temperature obtained from the equation (RA1 = 0.0008T°C + 0.3758) from Lahfid et al., (2010); T°C (RA2) = temperature obtained from the equation (RA2 = 0.0045T + 0.27) from Lahfid et al., (2010); wD/wG = full width at maximum height ratio between the D and G band; D-G distance = difference between G band and D band position, in cm^{-1}; Mean = average value calculated from 10 measurements; SD = standard deviation

Figure 1

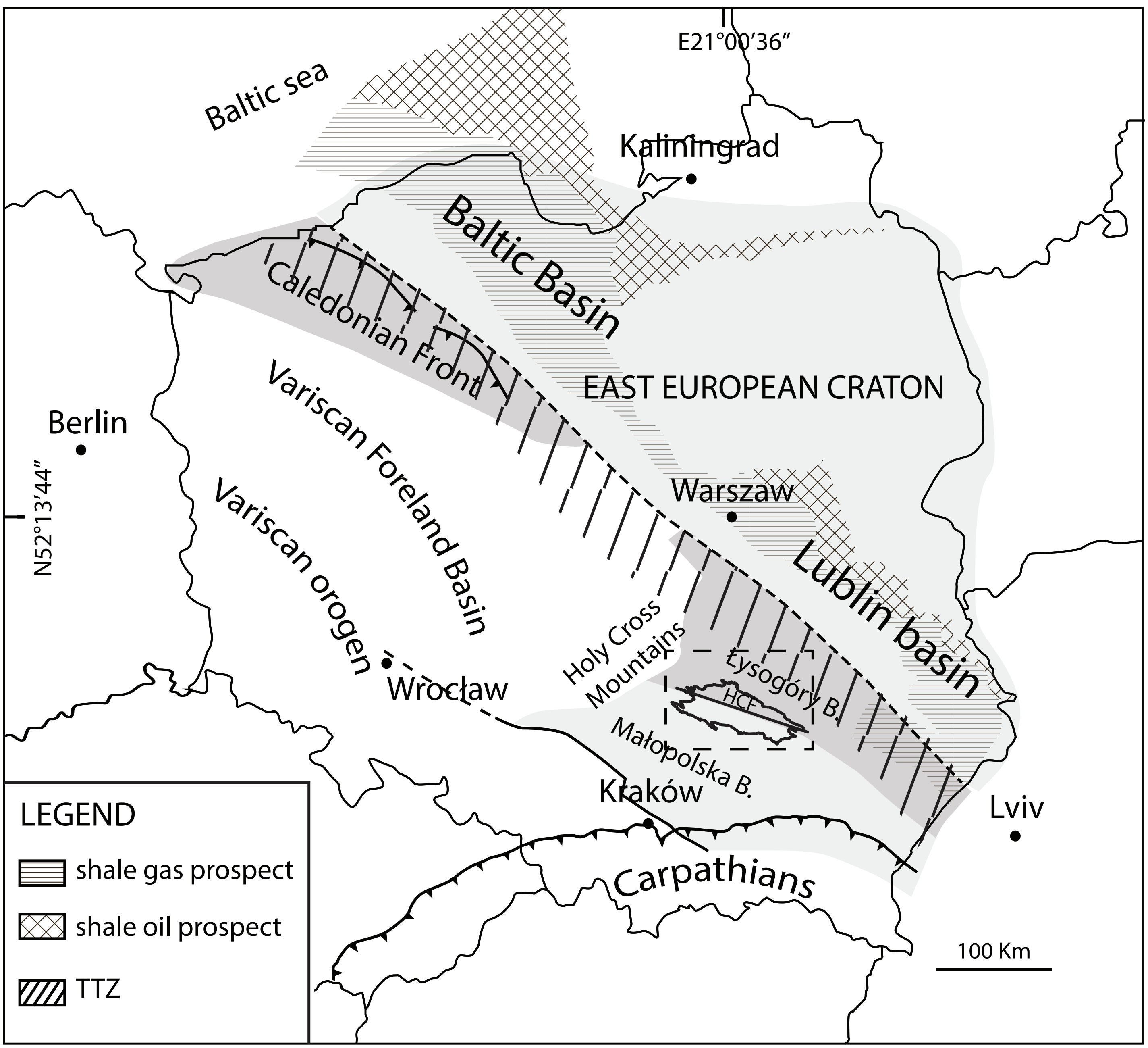
E21°00'36"
Baltic sea
Kaliningrad
Baltic Basin
Caledonian Front
EAST EUROPEAN CRATON
Berlin
Variscan Foreland Basin
Variscan orogen
N52°13'44"
Warszaw
Lublin basin
Holy Cross Mountains
Łysogóry B.
HCF
Małopolska B.
Wrocław
Kraków
Lviv
Carpathians
LEGEND
shale gas prospect
shale oil prospect
TTZ
100 Km

Figure 2

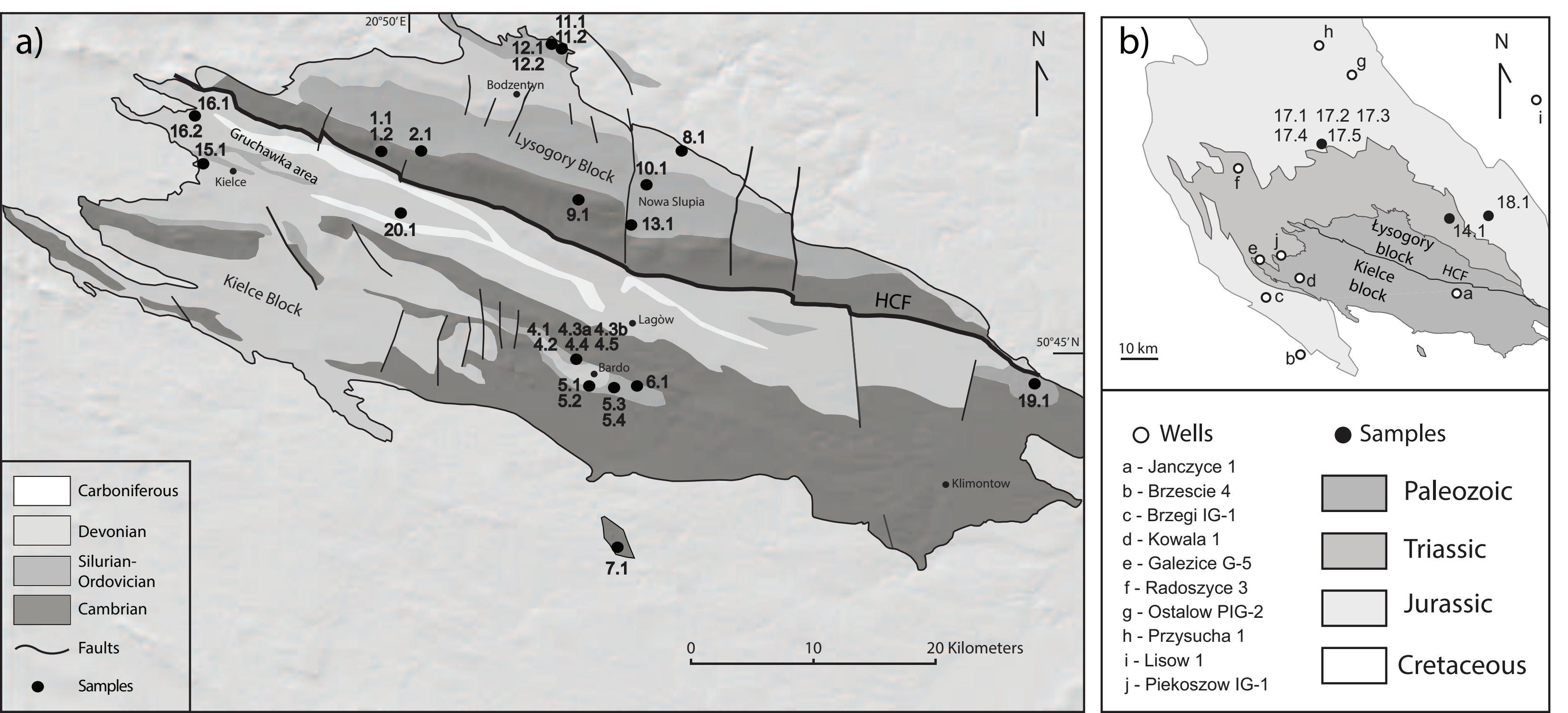
a)
b)
20°50'E
50°45'N
N
Lysogory Block
Kielce Block
Gruchawka area
HCF
Kielce
Bodzentyn
Nowa Slupia
Lagów
Bardo
Klimontow
1.1
1.2
2.1
8.1
9.1
10.1
11.1
11.2
12.1
12.2
13.1
15.1
16.1
16.2
19.1
20.1
4.1
4.2
4.3a
4.4
4.3b
4.5
5.1
5.2
5.3
5.4
6.1
7.1
Carboniferous
Devonian
Silurian-Ordovician
Cambrian
Faults
Samples
0
10
20 Kilometers
17.1 17.2 17.3
17.4 17.5
18.1
14.1
Łysogory block
Kielce block
10 km
Wells
Samples
a - Janczyce 1
b - Brzescie 4
c - Brzegi IG-1
d - Kowala 1
e - Galezice G-5
f - Radoszyce 3
g - Ostalow PIG-2
h - Przysucha 1
i - Lisow 1
j - Piekoszow IG-1
Paleozoic
Triassic
Jurassic
Cretaceous

Figure 3

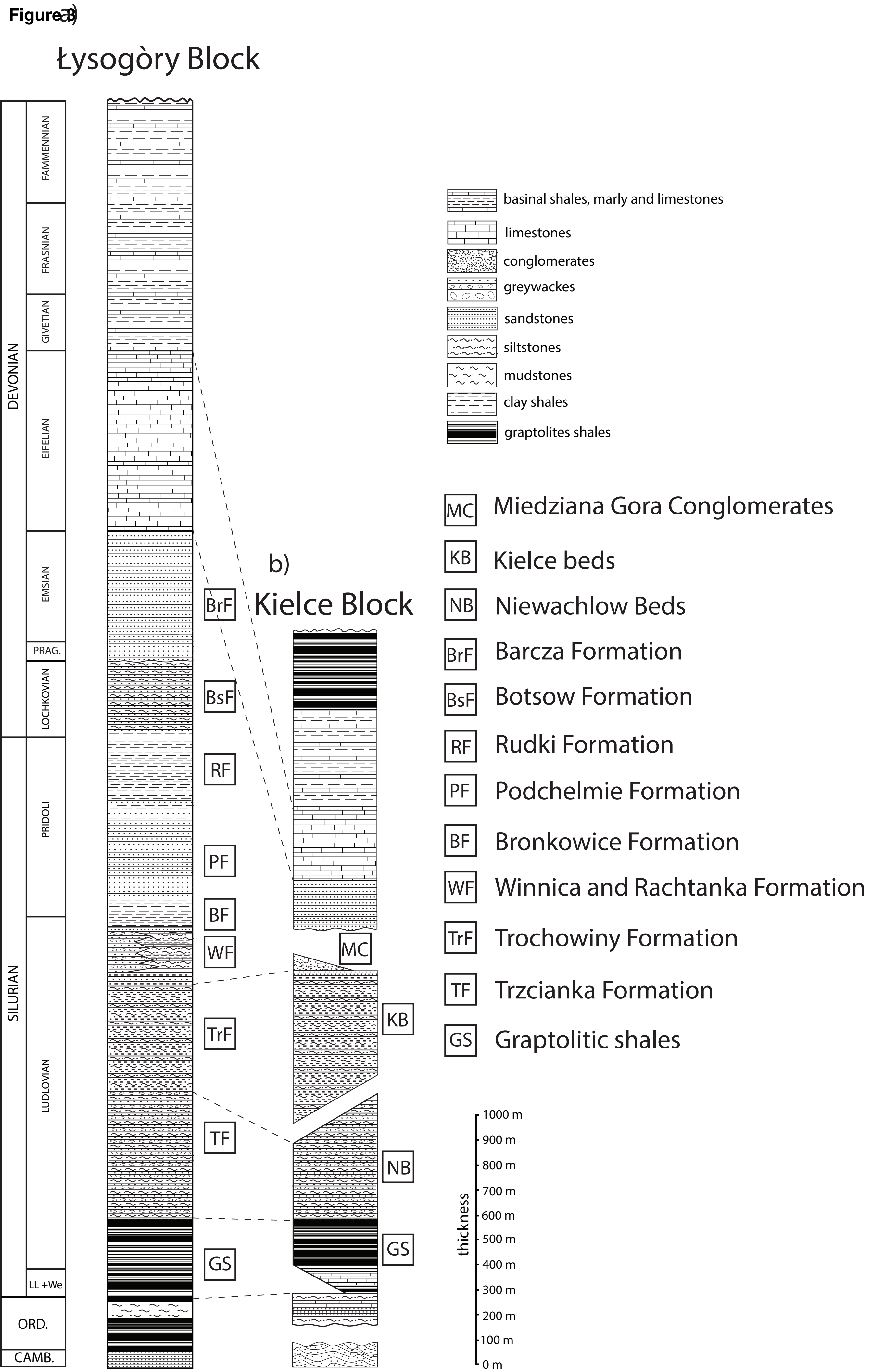
a)
Łysogòry Block
DEVONIAN
FAMMENNIAN
FRASNIAN
GIVETIAN
EIFELIAN
EMSIAN
PRAG.
LOCHKOVIAN
SILURIAN
PRIDOLI
LUDLOVIAN
LL +We
ORD.
CAMB.
BrF
BsF
RF
PF
BF
WF
TrF
TF
GS
b)
Kielce Block
MC
KB
NB
GS
basinal shales, marly and limestones
limestones
conglomerates
greywackes
sandstones
siltstones
mudstones
clay shales
graptolites shales
MC Miedziana Gora Conglomerates
KB Kielce beds
NB Niewachlow Beds
BrF Barcza Formation
BsF Botsow Formation
RF Rudki Formation
PF Podchelmie Formation
BF Bronkowice Formation
WF Winnica and Rachtanka Formation
TrF Trochowiny Formation
TF Trzcianka Formation
GS Graptolitic shales
thickness
1000 m
900 m
800 m
700 m
600 m
500 m
400 m
300 m
200 m
100 m
0 m

Figure 4

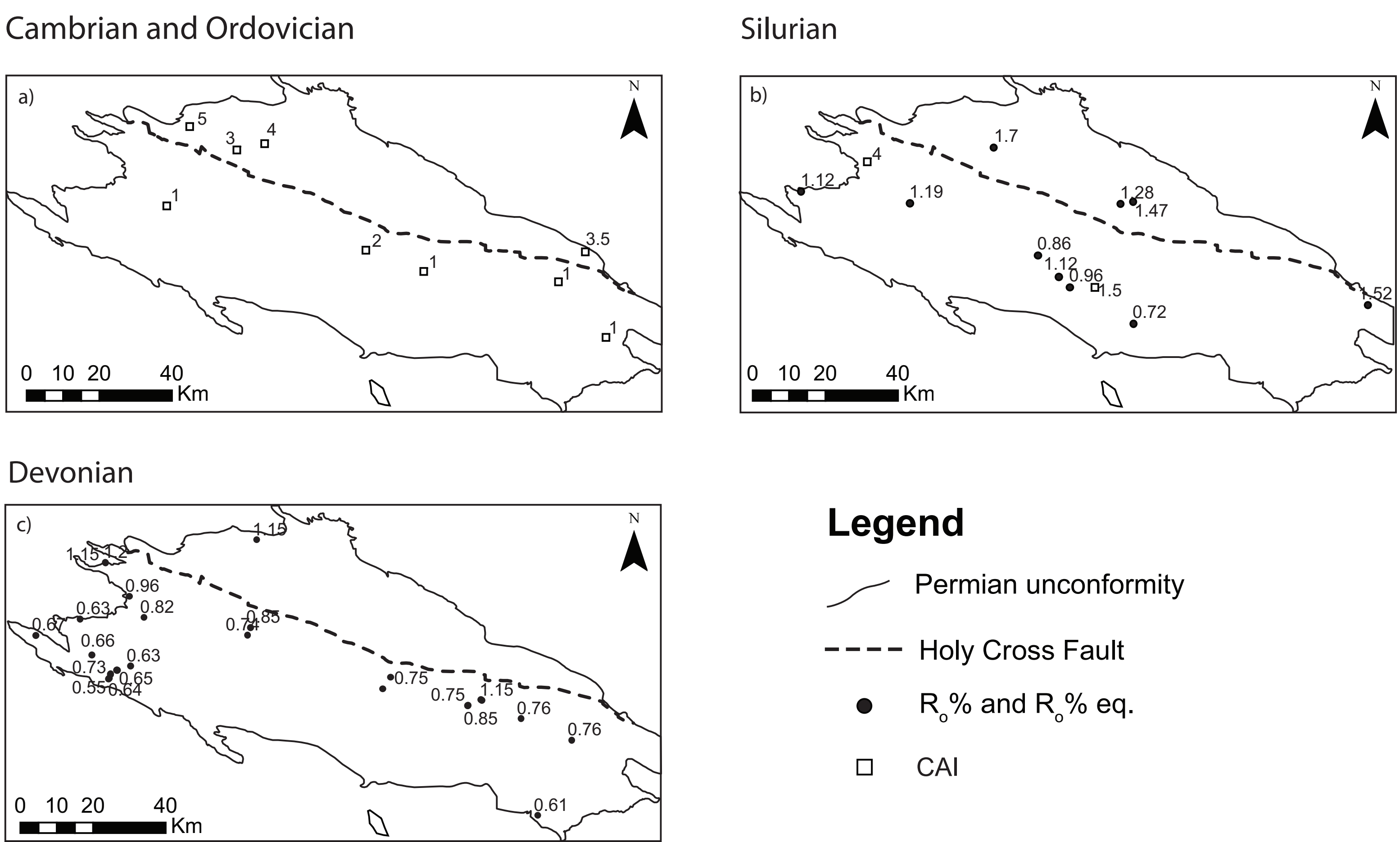

Cambrian and Ordovician
a)
N
5
3
4
1
2
1
3.5
1
1
0 10 20 40
Km
Silurian
b)
N
1.7
4
1.12
1.19
1.28
1.47
0.86
1.12
0.96
1.5
0.72
1.52
0 10 20 40
Km
Devonian
c)
N
1.15
1.15
1.2
0.96
0.63
0.82
0.67
0.74
0.85
0.66
0.63
0.73
0.65
0.55
0.64
0.75
0.75
1.15
0.85
0.76
0.76
0.61
0 10 20 40
Km
Legend
Permian unconformity
Holy Cross Fault
R_o% and R_o% eq.
CAI

Figure 5

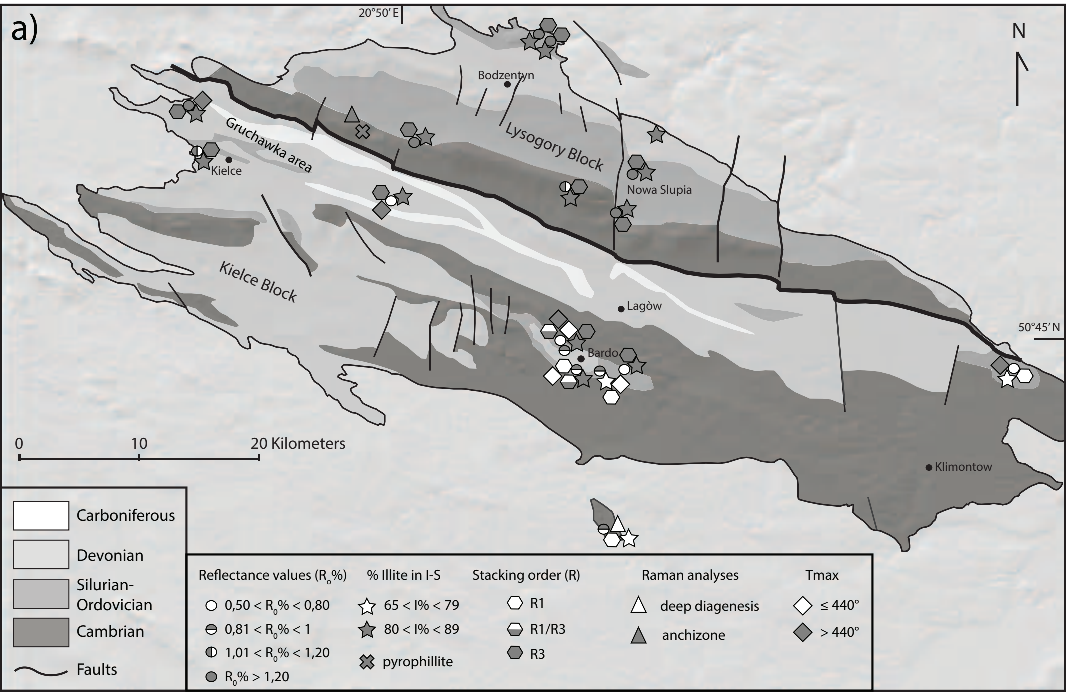
a)
20°50' E
N
Bodzentyn
Gruchawka area
Lysogory Block
Kielce
Nowa Slupia
Kielce Block
Lagòw
Bardo
50°45' N
Klimontow
0
10
20 Kilometers
Carboniferous
Devonian
Silurian-
Ordovician
Cambrian
Faults
Reflectance values (R0%)
0,50 < R0% < 0,80
0,81 < R0% < 1
1,01 < R0% < 1,20
R0% > 1,20
% Illite in I-S
65 < I% < 79
80 < I% < 89
pyrophillite
Stacking order (R)
R1
R1/R3
R3
Raman analyses
deep diagenesis
anchizone
Tmax
≤ 440°
> 440°

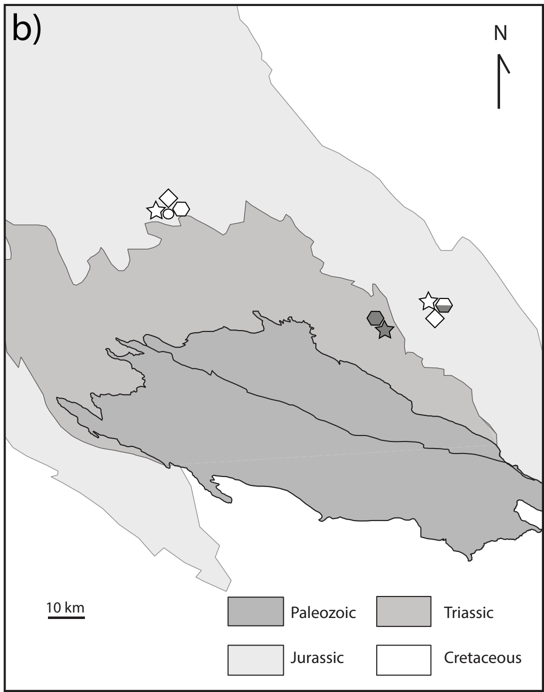
b)
N
10 km
Paleozoic
Triassic
Jurassic
Cretaceous

Figure 6

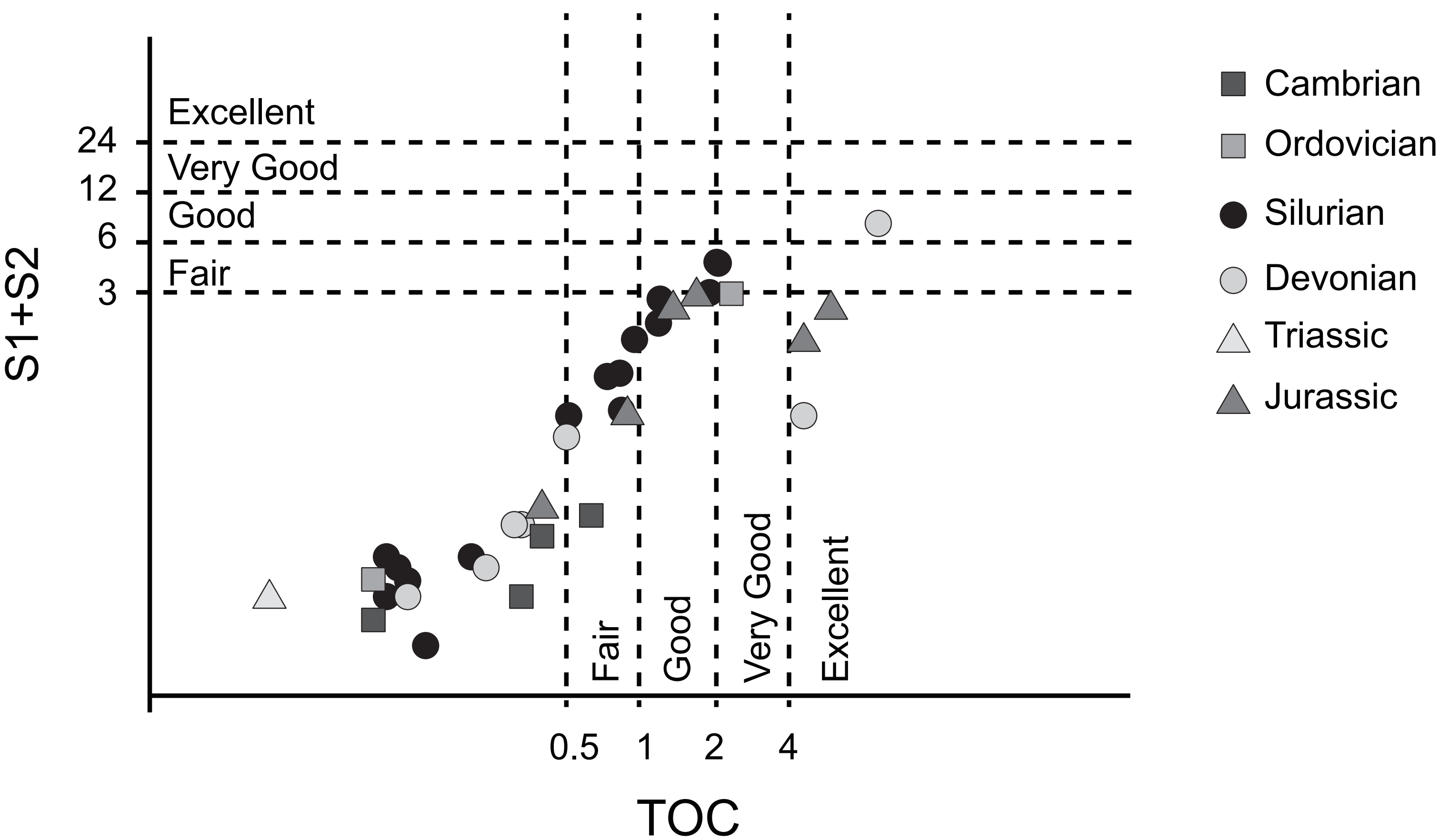

Excellent
Very Good
Good
Fair
24
12
6
3
S1+S2
Fair
Good
Very Good
Excellent
0.5
1
2
4
TOC
Cambrian
Ordovician
Silurian
Devonian
Triassic
Jurassic

Figure 7

a)

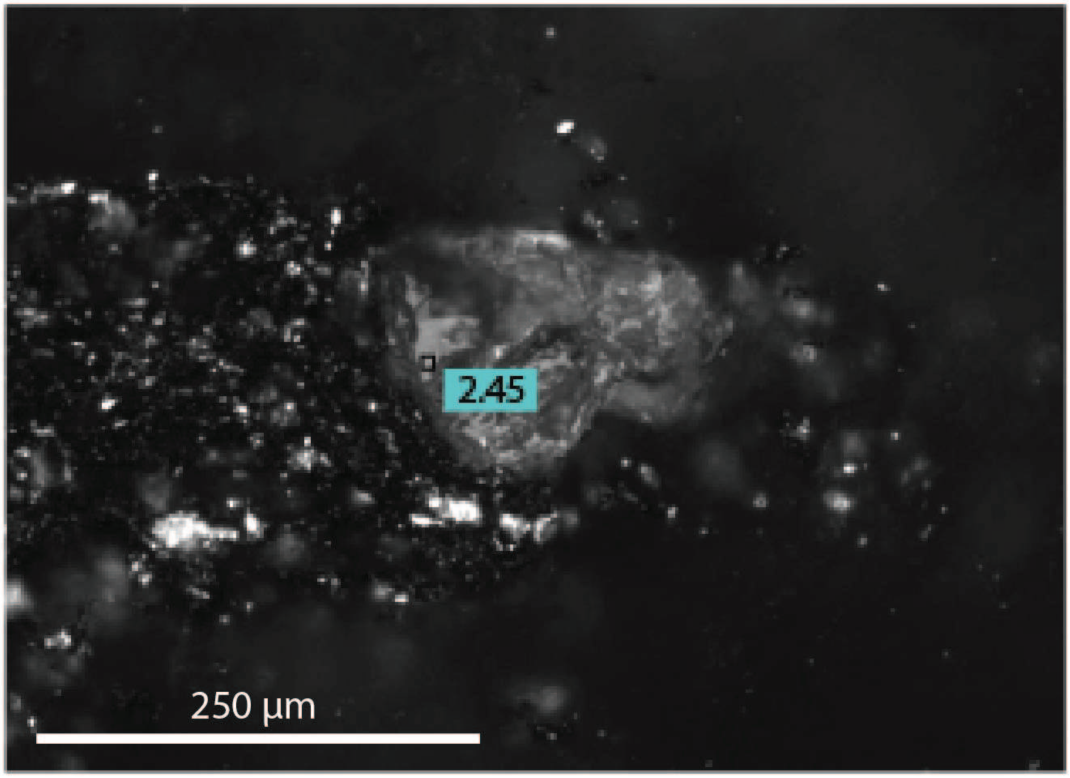

b)

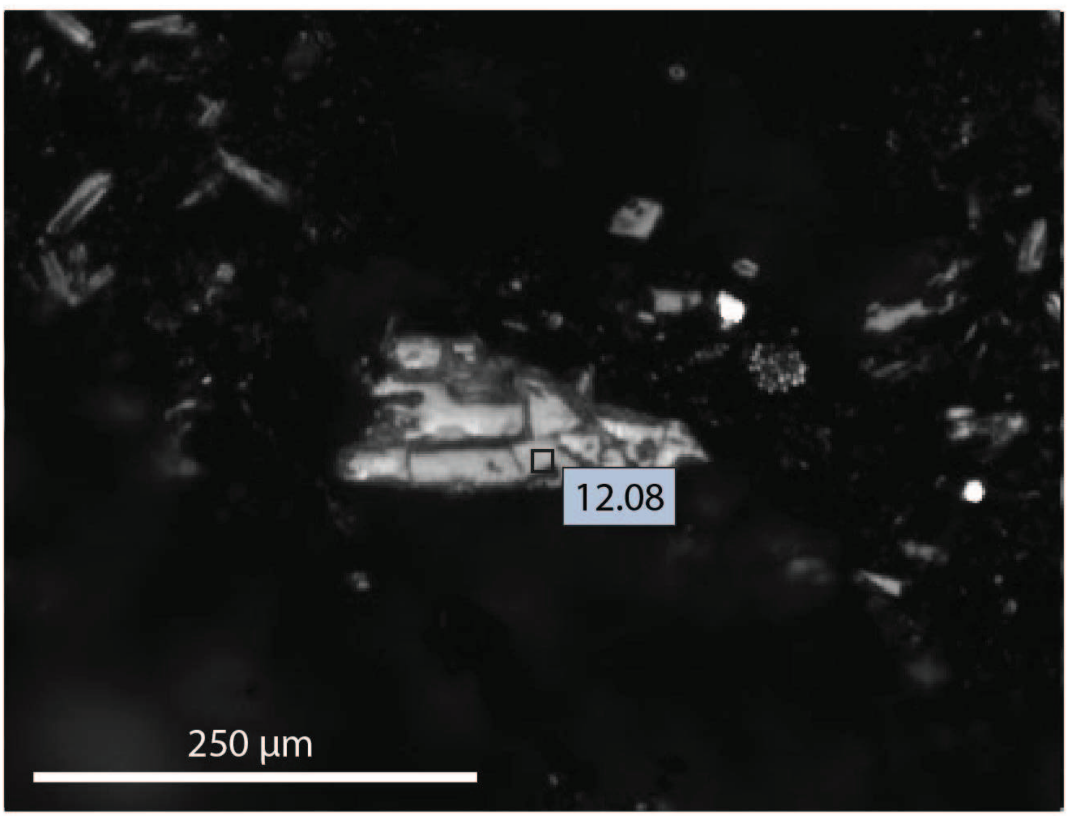

Figure 8
Click here to download high resolution image

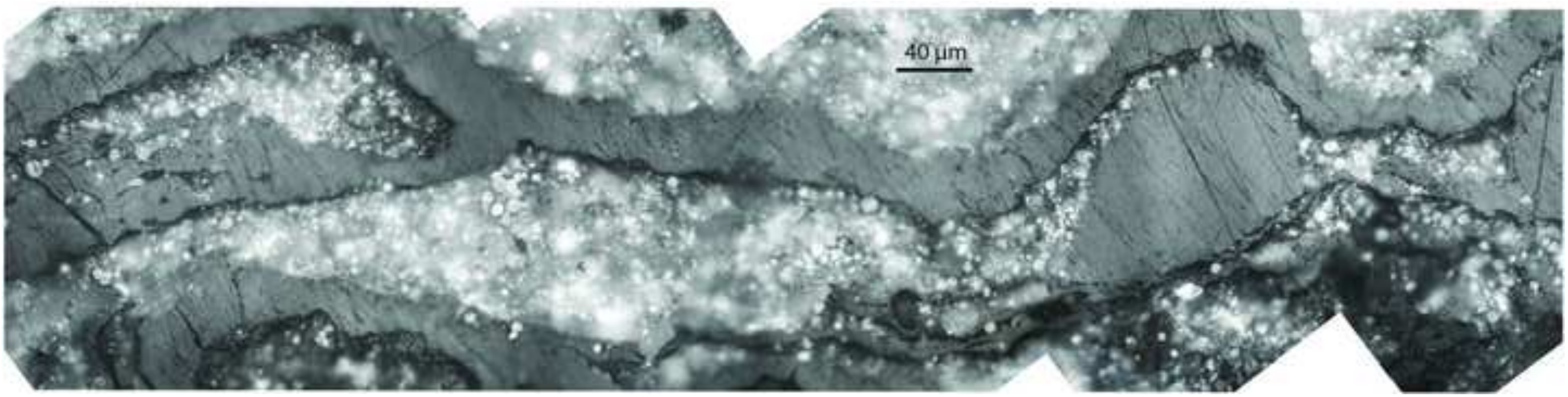

Figure 9

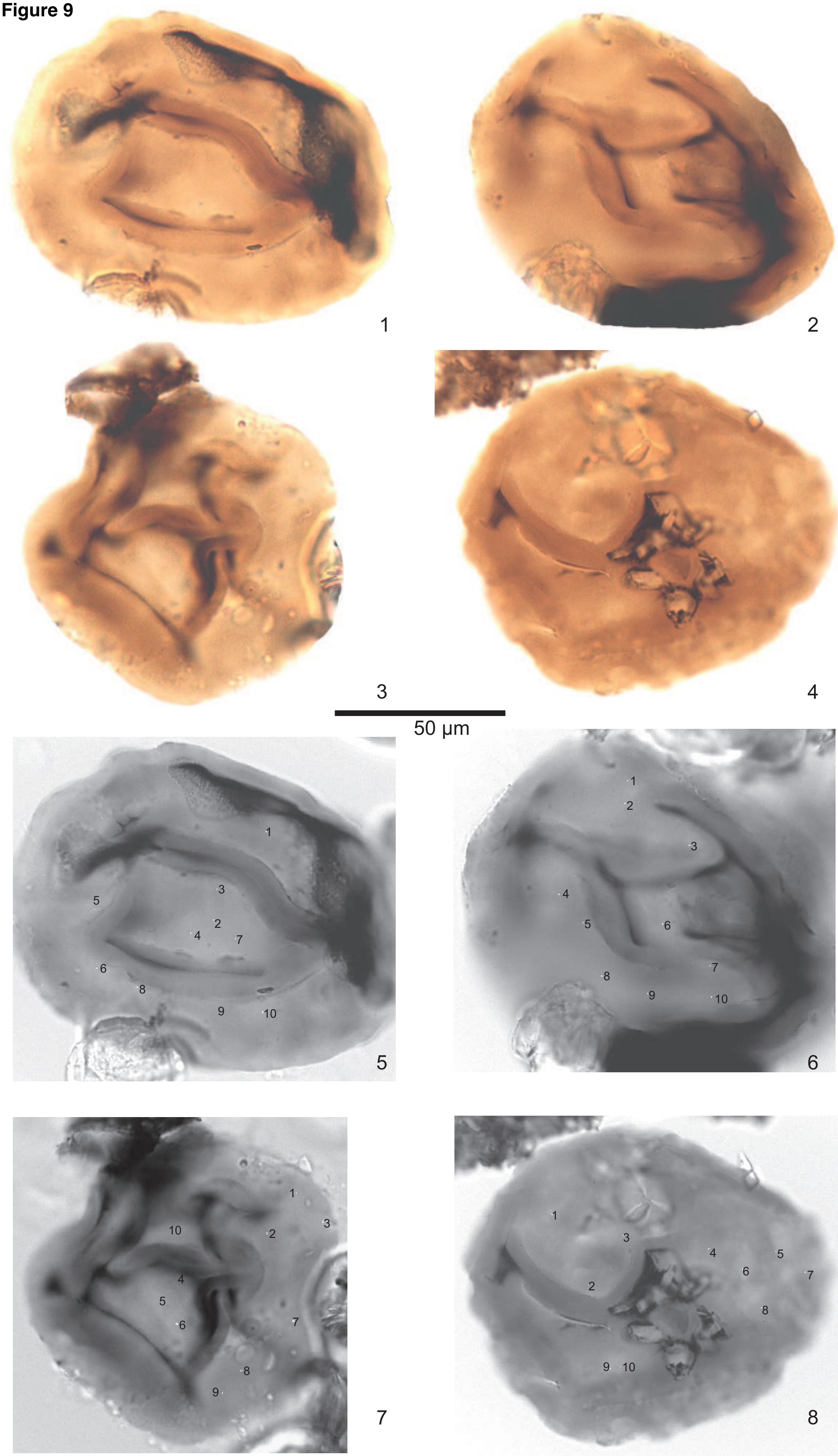

Figure 10

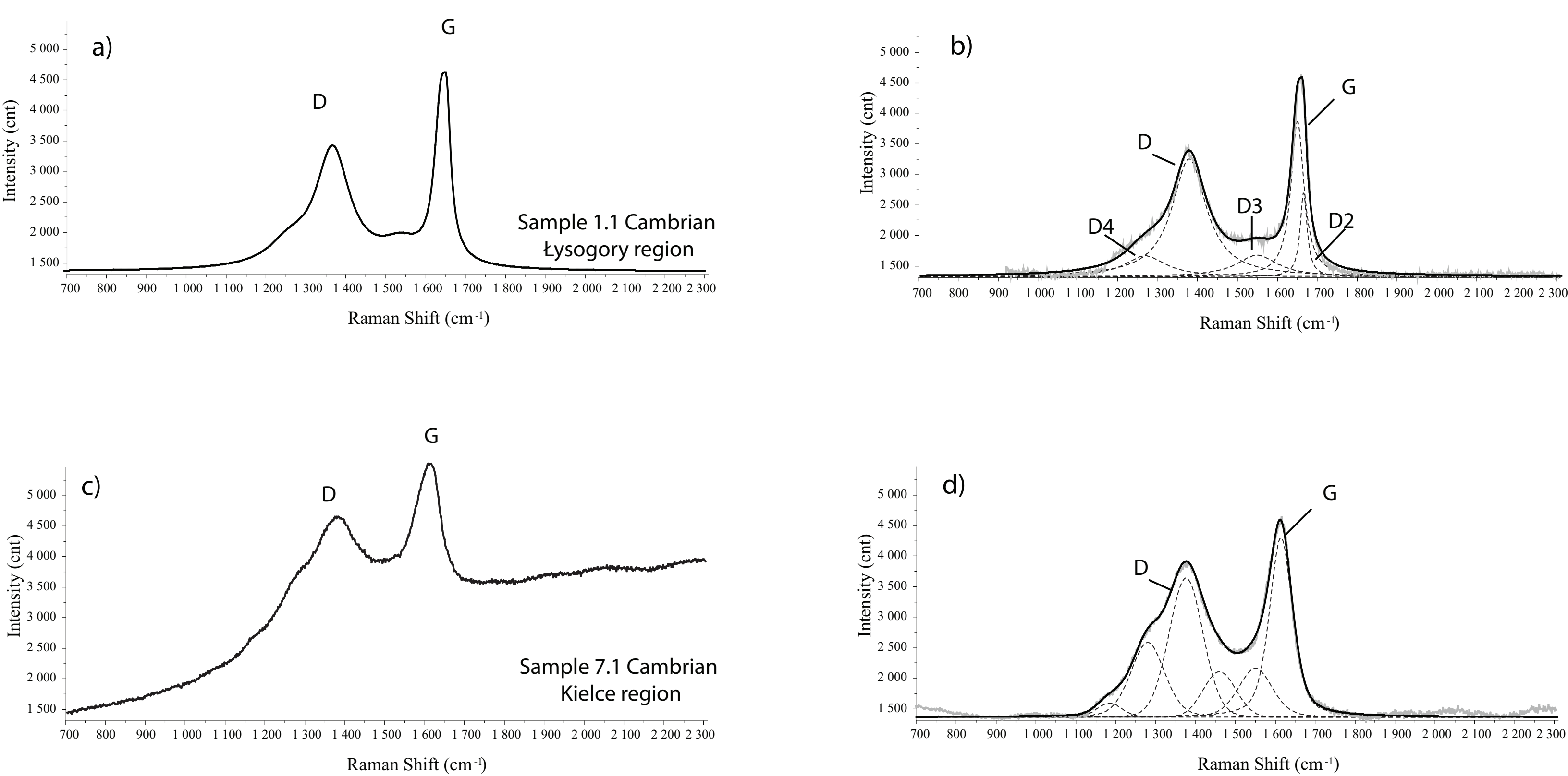

a)
D
G
Sample 1.1 Cambrian
Łysogory region
Intensity (cnt)
Raman Shift (cm⁻¹)
b)
D
G
D4
D3
D2
Intensity (cnt)
Raman Shift (cm⁻¹)
c)
D
G
Sample 7.1 Cambrian
Kielce region
Intensity (cnt)
Raman Shift (cm⁻¹)
d)
D
G
Intensity (cnt)
Raman Shift (cm⁻¹)

Figure 11

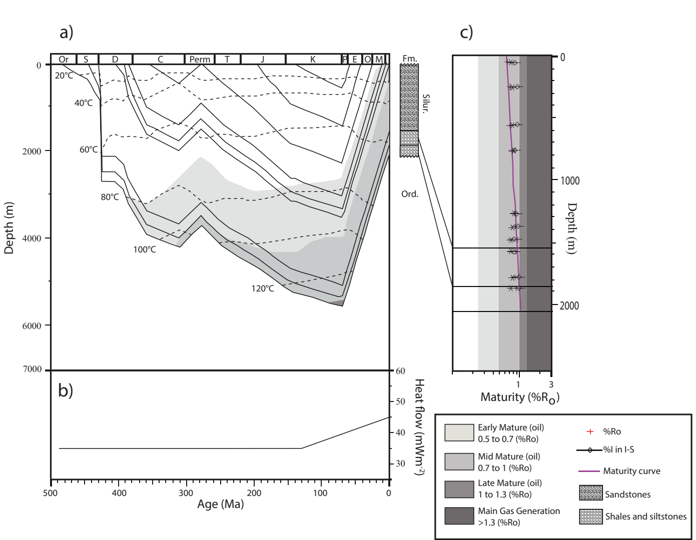
a)
Or
S
D
C
Perm
T
J
K
P
E
O
M
Fm.
Silur.
Ord.
20°C
40°C
60°C
80°C
100°C
120°C
Depth (m)
0
2000
4000
6000
7000
b)
Heat flow (mWm⁻²)
60
50
40
30
500
400
300
200
100
0
Age (Ma)
c)
Depth (m)
0
1000
2000
Maturity (%Ro)
1
3
Early Mature (oil) 0.5 to 0.7 (%Ro)
Mid Mature (oil) 0.7 to 1 (%Ro)
Late Mature (oil) 1 to 1.3 (%Ro)
Main Gas Generation >1.3 (%Ro)
%Ro
%I in I-S
Maturity curve
Sandstones
Shales and siltstones

Figure 12

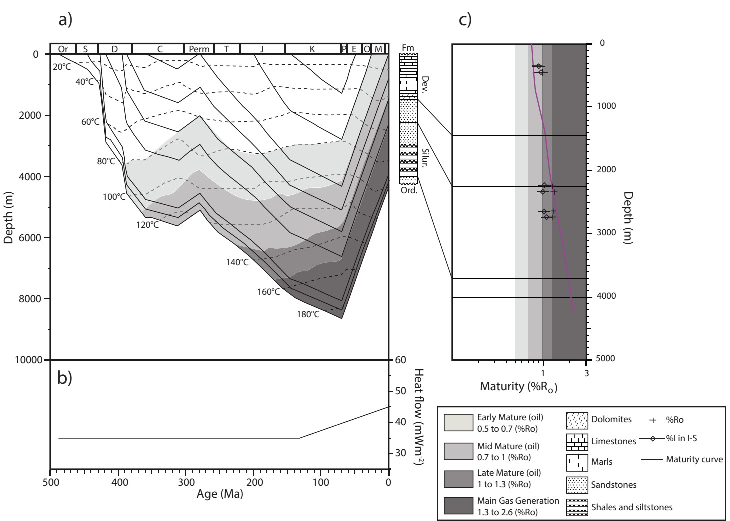

Figure 13

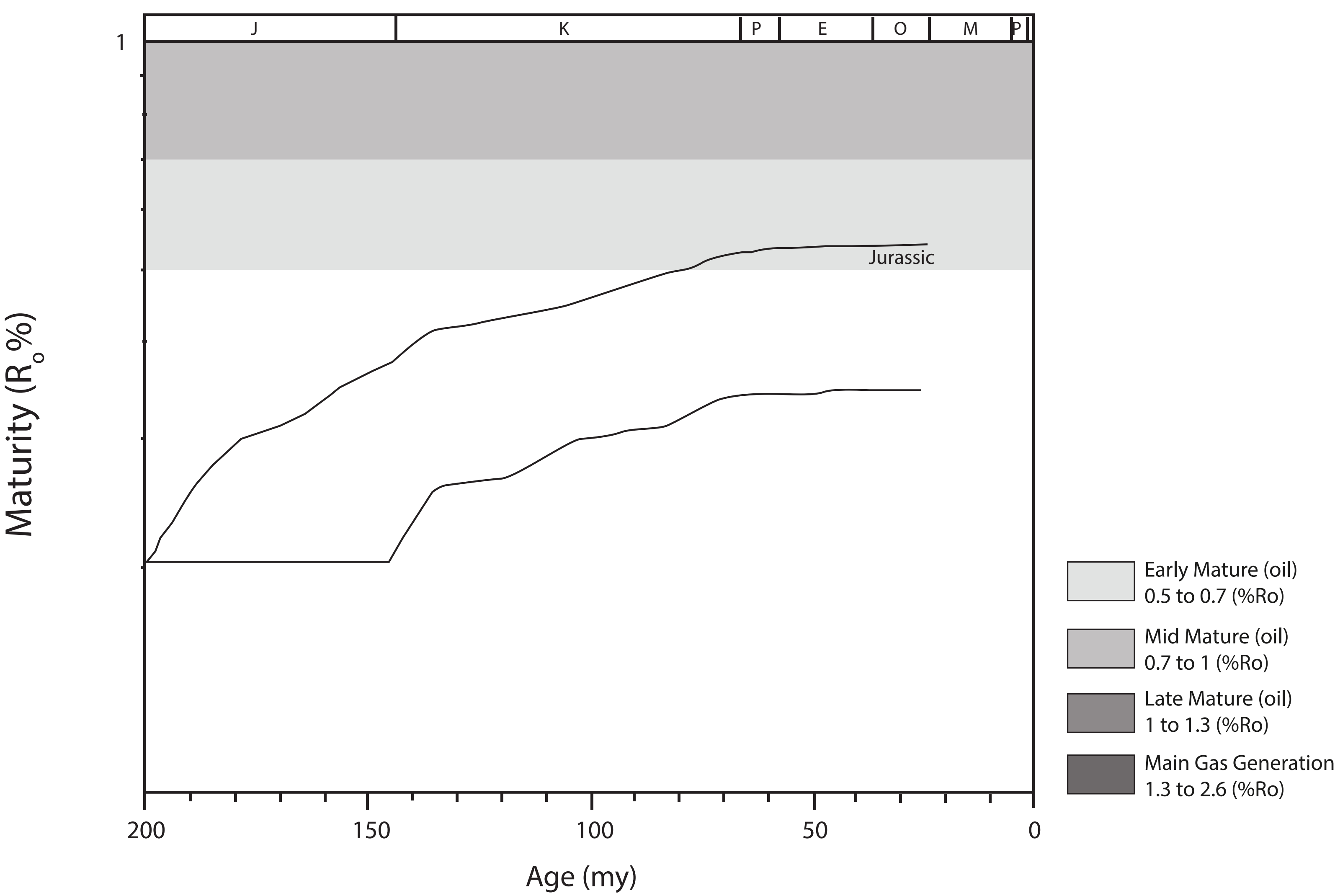

J
K
P
E
O
M
P
1
Jurassic
Maturity (R_o%)
200
150
100
50
0
Age (my)
Early Mature (oil)
0.5 to 0.7 (%Ro)
Mid Mature (oil)
0.7 to 1 (%Ro)
Late Mature (oil)
1 to 1.3 (%Ro)
Main Gas Generation
1.3 to 2.6 (%Ro)

Figure 14

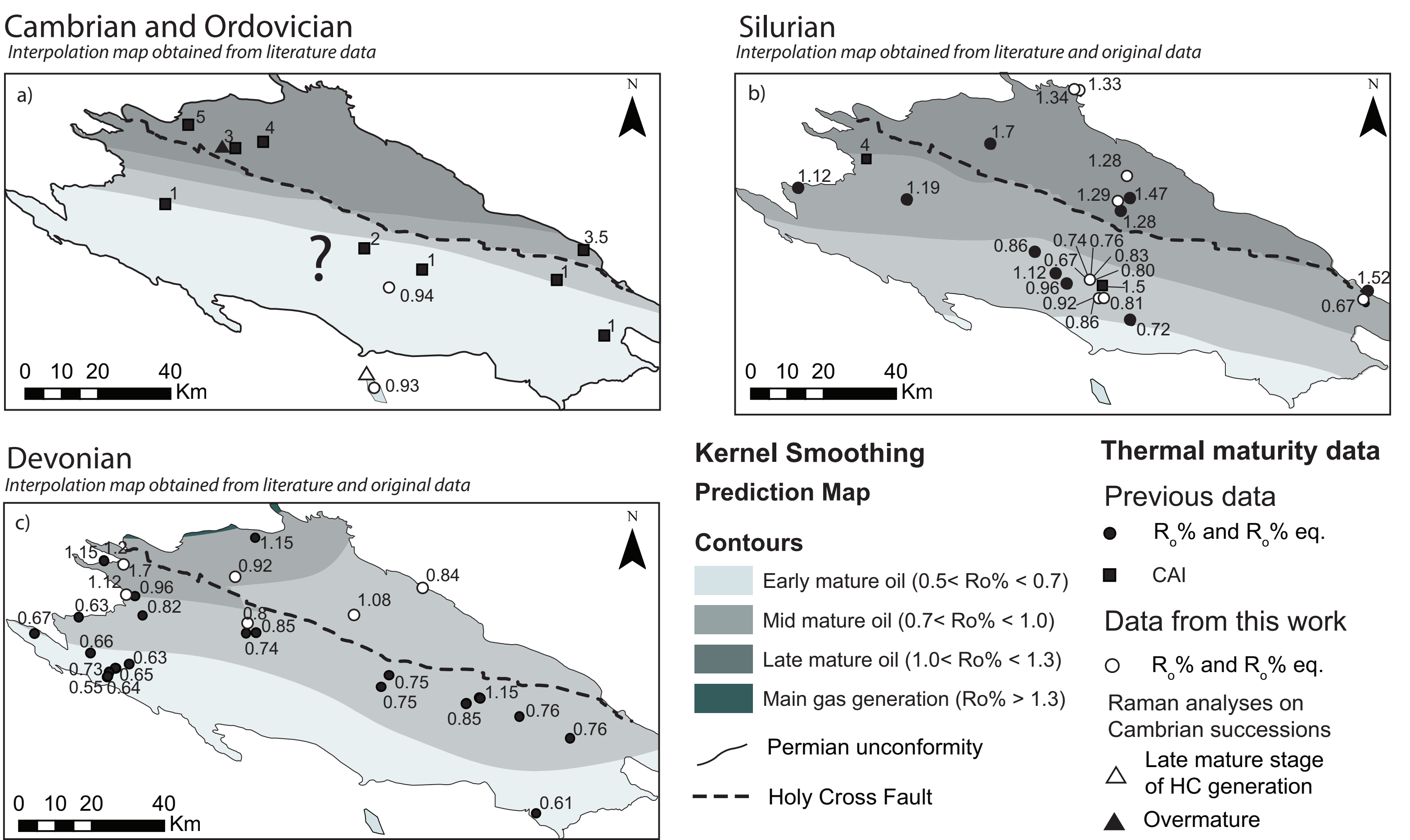

Cambrian and Ordovician
Interpolation map obtained from literature data
a)
5
3
4
1
3.5
2
?
1
1
0.94
1
0.93
0 10 20 40
Km
Silurian
Interpolation map obtained from literature and original data
b)
1.34
1.33
1.7
4
1.28
1.12
1.19
1.29
1.47
1.28
0.86
0.74
0.76
0.83
0.67
0.80
1.12
0.96
1.5
0.92
0.81
0.86
0.72
1.52
0.67
0 10 20 40
Km
Devonian
Interpolation map obtained from literature and original data
c)
1.15
1.2
1.15
1.7
0.92
0.84
1.12
0.96
0.63
0.82
1.08
0.67
0.8
0.85
0.74
0.66
0.63
0.73
0.65
0.55
0.64
0.75
0.75
1.15
0.85
0.76
0.76
0.61
0 10 20 40
Km
Kernel Smoothing
Prediction Map
Contours
Early mature oil (0.5< Ro% < 0.7)
Mid mature oil (0.7< Ro% < 1.0)
Late mature oil (1.0< Ro% < 1.3)
Main gas generation (Ro% > 1.3)
Permian unconformity
Holy Cross Fault
Thermal maturity data
Previous data
Ro% and Ro% eq.
CAI
Data from this work
Ro% and Ro% eq.
Raman analyses on
Cambrian successions
Late mature stage
of HC generation
Overmature

Figure 15

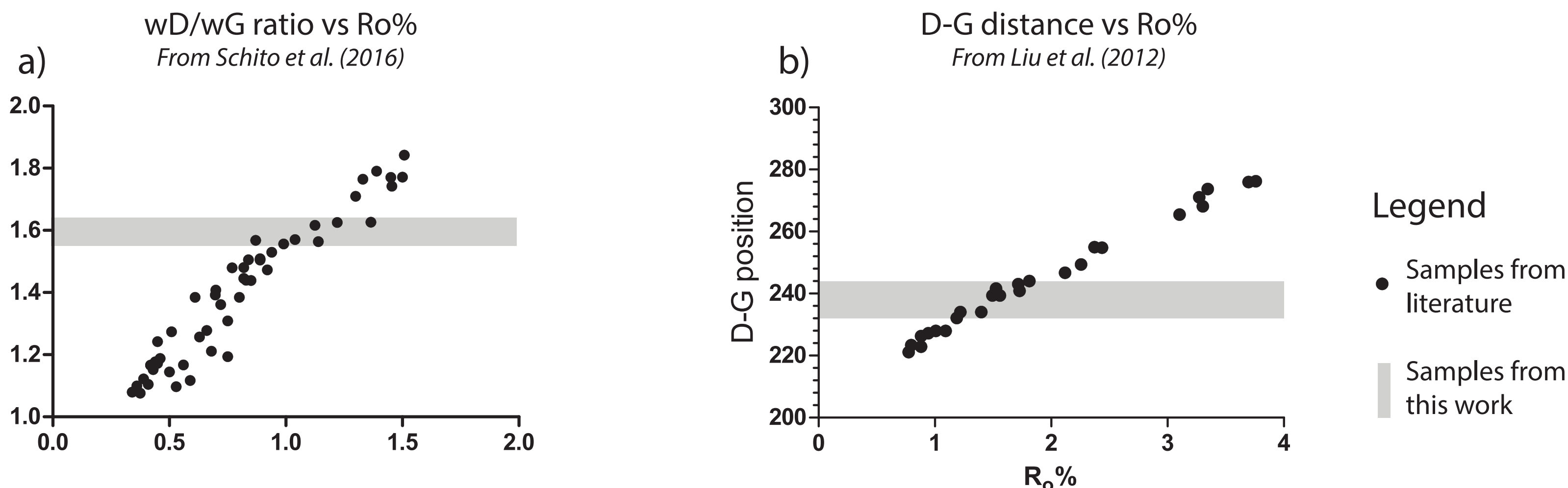

wD/wG ratio vs Ro%
a)
From Schito et al. (2016)
2.0
1.8
1.6
1.4
1.2
1.0
0.0
0.5
1.0
1.5
2.0
D-G distance vs Ro%
b)
From Liu et al. (2012)
D-G position
300
280
260
240
220
200
0
1
2
3
4
R_o%
Legend
Samples from literature
Samples from this work

Table 1

Samples	Coordinates (Lat-Long)	Formation	Age	Block	Lithologies
CAMBRIAN					
7.1	N50° 36' 24.2", E20° 04' 23.0"		Lower Cambrian	Kielce	Marl
1.1	N50° 53' 41.2", E20° 47' 24.5"		Upper Cambrian	Łysogory	Laminated shales
1.2	N50° 53' 43.9", E20° 47' 34.2"		Upper Cambrian	Łysogory	Laminated shales
ORDOVICIAN					
6.1	N50° 43' 13.3", E21° 04' 46.2"		Upper Ordovician	Kielce	Laminated shales
5.4	N50° 43' 27.4", E21° 03' 31.2"	Zalesie	Upper Ordovician	Kielce	Black shales
SILURIAN					
19.1	N50° 44' 24.8", E21° 33' 49.9"		Llandoverian	Kielce	Black shales
5.1	N50° 43' 27.5", E21° 03' 02.5"	Bardo	Llandoverian	Kielce	Silty shales
5.2	N50° 43' 27.5", E21° 03' 02.5"	Bardo	Llandoverian	Kielce	Silty shales
5.3	N50° 43' 28.4", E21° 03' 36.6"	Bardo	Llandoverian	Kielce	Silty shales
4.5	N50° 44' 46.8", E21° 02' 14.6"		Wenlock	Kielce	Silty shales
4.4	N50° 44' 43.3", E21° 02' 00.3"		Wenlock	Kielce	Marly clay
4.3b	N50° 44' 49.3", E21° 01' 58.0"		Ludlowian	Kielce	Marly clay
4.3a	N50° 44' 49.3", E21° 01' 58.0"		Ludlowian	Kielce	Marly clay
4.2	N50° 44' 49.4", E21° 01' 55.5"		Ludlowian	Kielce	Marly clay
4.1	N50° 44' 48.9", E21° 01' 50.5"		Ludlowian	Kielce	Silt
13.1	N50° 50' 34.8", E21° 05' 13.6"	Trzcianka	Ludlowian	Łysogory	Shales
12.1	N50° 58' 43.5", E21° 00' 11.9"	Trzcianka	Ludlowian	Łysogory	Silty shales
12.2	N50° 58' 43.5", E21° 00' 11.9"	Trzcianka	Ludlowian	Łysogory	Silty shales
11.1	N50° 58' 39.6", E21° 00' 46.3"	Trochowiny	Ludlowian	Łysogory	Shales
11.2	N50° 58' 39.6", E21° 00' 46.3"	Trochowiny	Ludlowian	Łysogory	Silty shales
10.1	N50° 52' 23.0", E21° 06' 15.7"	Winnica	Ludlowian	Łysogory	Silty shales
DEVONIAN					
8.1	N50° 53' 41.2", E21° 09' 30.6"		Eifelian	Łysogory	Marly clay
16.1	N50° 55' 24.5", E20° 34' 48.7"	Szydłówek	Givetian	Kielce	Marly clay
16.2	N50° 55' 24.5", E20° 34' 48.7"	Szydłówek	Givetian	Kielce	Marly limestones
9.1	N50° 51' 43.3", E21° 01' 32.1"		Givetian/	Łysogory	Silty shales
2.1	N50° 54' 30.6", E20° 47' 45.2"		Frasnian	Łysogory	Black shales
15.1	N50° 53' 11.3", E20° 35' 07.9"	Kostomłoty	Frasnian	Kielce	Marly clay
20.1	N50° 51' 07.9", E20° 49' 12.9"		Frasnian	Kielce	Marly limestones
TRIASSIC					
14.1	N50° 57' 38.1", E21° 11' 40.9"		Triassic	Łysogory	Arenite
JURASSIC					
17.1	N51° 08' 49.7", E20° 39' 41.3"		Hettangian	Łysogory	Arenite
17.2	N51° 08' 49.7", E20° 39' 41.3"		Hettangian	Łysogory	Black shales
17.3	N51° 08' 49.7", E20° 39' 41.3"		Hettangian	Łysogory	Shales
17.4	N51° 08' 49.7", E20° 39' 41.3"		Hettangian	Łysogory	Marly limestones
17.5	N51° 08' 49.7", E20° 39' 41.3"		Hettangian	Łysogory	Arenite
18.1	N50° 53' 30.2", E21° 21' 36.3"		Hettangian	Łysogory	Silty shales

Table 2

Samples	Whole-rock composition	<2µm grain size fraction	%I in I-S (R)	%C in C-S
CAMBRIAN				
7.1	Qtz_{13} Pl_{10} Ph_{76} Hem_{1}	I_{72} $I\text{-}S_{10}$ $C\text{-}S_{17}$ Chl_{1}	77 (R1-R3)	55
1.1	Qtz_{18} Kfs_{2} Pl_{4} Ph_{76}	I_{91} Rec_{5} Chl_{3} Prl_{1}	-	-
1.2	Qtz_{23} Kfs_{1} Pl_{3} Ph_{73}	I_{90} Rec_{3} Kln_{6} Prl_{1}	-	-
ORDOVICIAN				
6.1	Qtz_{23} Pl_{2} Ph_{73} Hem_{2}	I_{69} $I\text{-}S_{11}$ Kln_{20}	83 (R3)	-
5.4	Qtz_{33} Kfs_{1} Pl_{2} Ph_{64}	I_{59} $I\text{-}S_{20}$ Kln_{21}	83 (R3)	-
SILURIAN				
19.1	Qtz_{17} Pl_{3} Ph_{74} Gt_{6}	I_{87} $I\text{-}S_{7}$ Kln_{5} Chl_{1}	83 (R3)	-
5.1	Qtz_{40} Kfs_{1} Pl_{3} Ph_{56}	I_{72} $I\text{-}S_{15}$ Chl_{13}	77 (R1)	-
5.2	Qtz_{31} Kfs_{1} Pl_{6} Ph_{62}	I_{74} $I\text{-}S_{15}$ Chl_{11}	77 (R1)	-
5.3	Qtz_{14} Pl_{7} Ph_{79}	I_{85} $I\text{-}S_{1}$ $C\text{-}S_{9}$ Kln_{1} Chl_{4}	83 (R1-R3)	60
4.5	Qtz_{17} Kfs_{1} Pl_{7} Ph_{75}	I_{69} $I\text{-}S_{7}$ $C\text{-}S_{17}$ Kln_{3} Chl_{4}	83 (R3)	60
4.4	Qtz_{14} Cal_{4} Kfs_{1} Pl_{8} Ph_{69} Py_{2} Dol_{2}	I_{67} $I\text{-}S_{2}$ $C\text{-}S_{10}$ Kln_{4} Chl_{17}	81 (R3)	80
4.3b	Qtz_{17} Cal_{5} Kfs_{1} Pl_{9} Ph_{67} Dol_{1}	I_{65} $I\text{-}S_{2}$ $C\text{-}S_{8}$ Kln_{3} Chl_{22}	80 (R3)	80
4.3a	Qtz_{17} Cal_{6} Kfs_{1} Pl_{12} Ph_{62} Py_{1} Dol_{1}	I_{66} $I\text{-}S_{6}$ $C\text{-}S_{9}$ Kln_{5} Chl_{14}	82 (R3)	80
4.2	Qtz_{13} Cal_{2} Kfs_{1} Pl_{10} Ph_{74}	I_{55} $I\text{-}S_{12}$ $C\text{-}S_{12}$ Kln_{4} Chl_{17}	83 (R3)	80
4.1	Qtz_{12} Kfs_{1} Pl_{8} Ph_{79}	I_{64} $I\text{-}S_{19}$ $C\text{-}S_{14}$ Kln_{1} Chl_{2}	80 (R1-R3)	60
13.1	Qtz_{9} Pl_{2} Ph_{89}	Sm_{43} I_{50} $I\text{-}S_{2}$ Chl_{5}	88 (R3)	-
12.1	Qtz_{16} Pl_{6} Ph_{78}	I_{62} $I\text{-}S_{4}$ Chl_{34}	86 (R3)	-
12.2	Qtz_{15} Pl_{6} Ph_{79}	I_{62} $I\text{-}S_{8}$ $C\text{-}S_{11}$ Kln_{4} Chl_{15}	86 (R3)	54
11.1	Qtz_{5} Pl_{4} Ph_{88} Hem_{3}	I_{83} $I\text{-}S_{5}$ Kln_{10} Chl_{2}	85 (R3)	-
11.2	Qtz_{15} Pl_{4} Ph_{80} Hem_{1}	I_{79} $I\text{-}S_{12}$ Kln_{4} Chl_{5}	85 (R3)	-
10.1	Qtz_{15} Pl_{6} Ph_{79}	I_{58} $I\text{-}S_{24}$ $C\text{-}S_{10}$ Kln_{7} Chl_{1}	85 (R3)	78
DEVONIAN				
8.1	Qtz_{2} Cal_{25} Ank_{1} Ph_{72}	I_{76} $I\text{-}S_{16}$ Kln_{8}	83 (R3)	-
16.1	Qtz_{7} Cal_{25} Kfs_{1} Pl_{2} Ph_{65}	I_{79} $I\text{-}S_{7}$ Chl_{14}	82 (R3)	-
16.2	Qtz_{5} Cal_{52} Kfs_{1} Pl_{1} Ank_{5} Ph_{35} Py_{1}	N.D.	N.D.	N.D.
9.1	Qtz_{9} Pl_{2} Ph_{87} Hem_{2}	I_{59} $I\text{-}S_{6}$ Kln_{27} Chl_{8}	82 (R3)	-
2.1	Qtz_{10} Pl_{4} Ph_{86}	I_{95} $I\text{-}S_{1}$ $C\text{-}S_{3}$ Kln_{1}	84 (R3)	50
15.1	Qtz_{6} Cal_{48} Pl_{1} Ph_{45}	I_{85} $I\text{-}S_{15}$	85 (R3)	-
20.1	Qtz_{2} Cal_{75} Ph_{23}	I_{80} $I\text{-}S_{12}$ Chl_{8}	80 (R1-R3)	-
TRIASSIC				
14.1	Qtz_{34} Pl_{2} Ph_{58} Hem_{6}	I_{78} $I\text{-}S_{5}$ Kln_{14} Chl_{3}	80 (R3)	N.D.
JURASSIC				
17.1	Qtz_{86} Ph_{14}	N.D.	N.D.	N.D.
17.2	Qtz_{2} Pl_{1} Ph_{97}	N.D.	N.D.	N.D.
17.3	Qtz_{15} Pl_{1} Ph_{84}	I_{38} $I\text{-}S_{26}$ Kln_{25} Chl_{11}	65 (R1)	-
17.4	Qtz_{69} Ph_{31}	N.D.	N.D.	N.D.
17.5	Qtz_{72} Kfs_{1} Ph_{27}	N.D.	N.D.	N.D.
18.1	Qtz_{10} Kfs_{1} Pl_{4} Ph_{84} Sd_{1}	I_{15} $I\text{-}S_{3}$ Kln_{68} Chl_{14}	75 (R1-R3)	-

Table 3

Samples	TOC (Wt%)	S1 (mg/g)	S2 (mg/g)	HI	Tmax
CAMBRIAN					
7.1	0.08	0.01	0.02	25	N.D.
1.1	0.31	0.02	0.02	6	N.D.
1.2	0.60	0.07	0.06	10	N.D.
ORDOVICIAN					
6.1	0.08	0.01	0.04	50	N.D.
5.4	2.31	0.03	2.92	126	439
SILURIAN					
19.1	0.82	0.02	0.53	65	442
5.1	2.01	0.09	4.36	217	439
5.2	2.04	0.10	4.28	210	437
5.3	1.88	0.09	2.81	149	440
4.5	0.81	0.09	0.84	104	441
4.4	1.16	0.16	1.72	148	442
4.3b	1.18	0.28	2.36	200	441
4.3a	0.93	0.15	1.35	145	441
4.2	0.72	0.10	0.79	110	439
4.1	0.50	0.10	0.41	82	441
13.1	0.2	0.02	0.05	25	N.D.
12.1	0.09	0.02	0.02	22	N.D.
12.2	0.09	0.04	0.03	33	N.D.
11.1	0.11	0.01	0.04	36	N.D.
11.2	0.10	0.02	0.04	40	N.D.
10.1	0.13	0.01	0.01	8	N.D.
DEVONIAN					
8.1	0.23	0.01	0.05	22	N.D.
16.1	4.57	0.10	0.41	9	N.D.
16.2	9.17	1.27	6.42	70	476
9.1	0.11	0.01	0.03	27	N.D.
2.1	0.32	0.06	0.05	16	N.D.
15.1	0.30	0.01	0.10	33	N.D.
20.1	0.49	0.03	0.35	71	441
TRIASSIC					
14.1	0.03	0.02	0.02	67	N.D.
JURASSIC					
17.1	0.39	0.01	0.13	33	N.D.
17.2	4.72	0.01	1.50	32	439
17.3	0.87	0.01	0.52	60	439
17.4	1.33	0.01	2.36	177	438
17.5	1.66	0.02	2.87	173	437
18.1	5.89	0.04	2.25	38	433

Table 4

Samples	R_{org}%	SD	R_0 %	SD	Nr. Meas	R_0% eq.		
						1	2	3
CAMBRIAN								
7.1	1.06	0.20	-	-	8	1.33	0.93	1.34
1.1	> 2	N.D.	-	-	N.D.	N.D.	N.D.	N.D.
1.2	> 2	N.D.	-	-	N.D.	N.D.	N.D.	N.D.
ORDOVICIAN								
6.1	0.86	N.D.	-	-	1	1.27	0.79	1.16
5.4	1.07	0.05	-	-	45	1.33	0.94	1.35
SILURIAN								
19.1	0.70	0.09	-	-	25	1.09	0.67	0.85
5.1	1.04	0.17	-	-	46	1.32	0.92	1.32
5.2	0.96	0.11	-	-	53	1.30	0.86	1.25
5.3	0.89	0.12	-	-	21	1.28	0.81	1.18
4.4	0.92	0.10	-	-	86	1.29	0.83	1.21
4.5	0.88	0.12	-	-	16	1.28	0.80	1.17
13.1	1.55	0.08	-	-	13	1.44	1.29	0.84
4.3b	0.95	0.14	-	-	89	1.30	0.85	1.24
4.3a	0.82	0.09	-	-	83	1.26	0.76	1.12
4.2	0.80	0.09	-	-	50	1.25	0.74	1.10
4.1	0.69	0.07	-	-	17	1.08	0.66	0.84
11.1	N.D.	N.D.	-	-	N.D.	N.D.	N.D.	N.D.
11.2	1.62	0.08	-	-	7	1.49	1.34	N.D.
10.1	1.68	0.17	-	-	45	1.42	1.28	N.D.
12.1	1.60	0.01	-	-	3	1.48	1.33	
12.2	N.D.	N.D.	-	-	N.D.	N.D.	N.D.	N.D.
DEVONIAN								
16.1	-	-	1.70	0.16	18			
16.2	-	-	1.95	0.09	4			
20.1	-	-	0.80	N.D.	1			
9.1	-	-	1.08	0.11	7			
2.1	-	-	0.92	0.04	18			
15.1	-	-	1.12	0.02	2			
8.1	-	-	0.84	0.14	54			
TRIASSIC								
14.1	-	-	N.D.	N.D.	N.D.	-	-	-
JURASSIC								
17.1	-	-	0.51	0.03	23	-	-	-
17.2	-	-	N.D.	N.D.	N.D.	-	-	-
17.3	-	-	0.57	0.07	9	-	-	-
17.4	-	-	N.D.	N.D.	N.D.	-	-	-
17.5	-	-	N.D.	N.D.	N.D.	-	-	-
18.1	-	-	0.57	0.06	47	-	-	-

Table 5

Lysogory region								
	RA1 parameter		RA2 parameter		T°C (RA1)		T°C (RA2)	
Age of Samples	Mean	SD	Mean	SD	Mean	SD	Mean	SD
Upper Cambrian	0.59	0.009	1.44	0.053	268.46	11.03	260.80	11.8
Kielce region								
	wD/wG				D-G distance			
Age of Samples	Mean		SD		Mean		SD	
Lower Cambrian	1.60		0.049		238.55		6.45	